The zinc finger transcription factor Gli3 is a regulator of precerebellar neuronal migration

Erick Martinez-Chavez[1], Claudia Scheerer[1§], Andrea Wizenmann[2], Sandra Blaess[1*]

[1]Institute of Reconstructive Neurobiology, University of Bonn Medical Center, 53127 Bonn, Germany

[2] Institute of Clinical Anatomy and Cell Analysis, Department of Anatomy, University of Tübingen, Tübingen, Germany

[§]Current address: CHKilger Anwaltspartnerschaft mbB, Fasanenstraße 29, 10719 Berlin, Germany

*Corresponding author, email: sblaess@uni-bonn.de

Key words: hindbrain, inferior olive, pontine nucleus, trigeminal ganglia, sonic hedgehog

SUMMARY STATEMENT

Gli3 plays an important, non-cell autonomous role in maintaining the organization of the precerebellar migratory streams and the final positioning of precerebellar neurons.

ABSTRACT

Hindbrain precerebellar neurons arise from progenitor pools at the dorsal edge of the embryonic hindbrain, the caudal rhombic lip. These neurons follow distinct migratory routes to establish nuclei that provide climbing or mossy fiber inputs to the cerebellum. *Gli3*, a zinc transcription factor in the Sonic hedgehog signaling pathway, is an important regulator of dorsal brain development. We demonstrate that in *Gli3* null mutant mice disrupted neuronal migratory streams lead to a disorganization of precerebellar nuclei. Precerebellar progenitors are properly established in *Gli3* null embryos and using conditional gene inactivation, we provide evidence that *Gli3* does not play a cell-autonomous role in migrating precerebellar neurons. Thus, Gli3 likely regulates the development of other hindbrain structures, such as non-precerebellar nuclei or cranial ganglia and their respective projections, which may in turn influence precerebellar migration. While the organization of non-precerebellar hindbrain nuclei appears to be largely unaffected in absence of *Gli3*, trigeminal ganglia and their central descending tracts are disrupted. We show that rostrally migrating precerebellar neurons are normally in close contact with these tracts, but are detached in *Gli3* null embryos.

INTRODUCTION

The hindbrain precerebellar system is divided into the mossy fiber (MF) and the climbing fiber (CF) system, based on the type of afferent connection with the cerebellum. Projections of the MF system terminate in cerebellar glomeruli where they form synapses with cerebellar granule cells and Golgi cells. CFs terminate on the dendrites of Purkinje cells. Both, MF and CF fibers also form collateral projections to the deep cerebellar nuclei (Paxinos, 2004). Anatomically, the hindbrain precerebellar system comprises bilaterally symmetrical pairs of nuclei situated in the hindbrain. There are four major MF nuclei: the external cuneate nuclei (ECN) and the lateral reticular nuclei (LRN) in the caudolateral hindbrain and the pontine nuclei (PN) and the reticulotegmental nuclei (RTN) in the rostroventral hindbrain. The inferior olivary nuclei (ION) in the caudoventral hindbrain are the one pair of CF nuclei (Watson 2012, schematic in **Fig. 1**).

Hindbrain precerebellar neurons originate from the rhombic lip (RL), a neuroepithelium in the dorsalmost part of the hindbrain that rims the opening of the fourth ventricle (Ray and Dymecki, 2009; Wingate, 2001). The RL extends along the entire rostrocaudal axis of the hindbrain, from rhombomere 1 to rhombomere 8 (r1-r8) (Liu et al., 2010; Ray and Dymecki, 2009; Storm et al., 2008). Anatomically, it can be divided into the upper RL (uRL in r1) and the lower RL (lRL in r2-r8). The uRL contains the progenitors of cerebellar granule neurons, unipolar brush cells and a subset of deep nuclei neurons (Englund et al., 2006; Machold and Fishell, 2005; Wang et al., 2005). The lRL is further subdivided: progenitors at the r2-r5 level contribute neurons to the cochlear nucleus, while the caudal lRL (clRL, r6-r8) gives rise to precerebellar MF neurons (MFN) and CF neurons (CFN) (Farago et al., 2006, Ray and Dymecki, 2009).

In the murine hindbrain, MFN and CFN emanate from the clRL between embryonic day (E)10 and E16 and undergo a long-distance migration to reach their final position. MFN migrate just beneath the pial surface in the anterior and posterior extramural stream (AES and PES). The AES turns rostrally after an initial step of ventrally-oriented migration, and moves through r5/r4, passing the vestibulocochlear and facial nerve roots. Once the AES reaches the trigeminal nerve root, it turns ventrally and the majority of AES neurons stop at the ipsilateral side of the ventral midline to form the PN/RTN. Neurons in the PES migrate ventrally, cross the midline and move dorsally to establish the LRN and ECN on the contralateral site. CFNs migrate in an intramural migrating stream (IMS), which is directed ventrally and eventually forms the ION (schematic in **Fig. S1**). Most CFNs stop at the ventral midline and their cell bodies remain ipsilateral to their progenitor domain. CFNs are the first to reach the ventral midline (around E13.5). The last neurons to settle are the MFNs that form the PN (up to E18.5) (Bloch-Gallego et al., 2005; Kratochwil et al., 2017; Shinohara et al., 2013). The distinctive migratory routes of these neurons are severely altered in absence

of guidance factors such as SLITs, Netrin and the chemokine CXCL12 (C-X-C motif chemokine 12) (Di Meglio et al., 2008; Dominici et al., 2018; Geisen et al., 2008; Gilthorpe et al., 2002; Kim and Ackerman, 2011; Kuwako et al., 2010; Marillat et al., 2004; Moreno-Bravo et al., 2018; Zhu et al., 2009). However, it is not completely decoded how the multi-step migration process of the precerebellar neurons is regulated.

Here we show that the zinc finger transcription factor Gli3, a transcriptional repressor in the Sonic hedgehog signaling pathway, plays an important role in maintaining the organization of the precerebellar migratory streams and the final positioning of precerebellar neurons. In particular, Gli3 is essential for the rostral migration of the r7/r8-derived subset of the AES and for the formation of a properly sized and organized ION. Using conditional gene inactivation of *Gli3*, we demonstrate that defects in precerebellar neuron migration and nuclei development are not dependent on a cell-autonomous function of Gli3 in MFN progenitors or neurons and that inactivation of *Gli3* in the central nervous system (CNS) after E10.5 does not alter the formation of the precerebellar system. These results suggest that the abnormal migratory path of precerebellar neurons in *Gli3 null* mutants could be caused (1) by early developmental patterning defects in non-clRL-derived hindbrain nuclei and their projections or (2) by aberrant development of tracts originating from non-CNS derived neuronal clusters, i.e. the cranial ganglia. These structures may normally act as a orienting substrate for the migrating precerebellar neurons. We provide indirect evidence that the descending tract of the trigeminal ganglia (spinal trigeminal tract; sp5) could potentially serve such a role. In controls, the AES is in close contact with the sp5 during its rostral-oriented migration phase. In *Gli3* null mutants, the sp5 is defasciculated and the AES is detached from the tract. In contrast, the organization of non-precerebellar hindbrain nuclei, appears to be largely unaffected in absence of *Gli3*. Further investigation will be required to determine whether the sp5 does indeed act as a guiding structure for precerebellar migration and whether and which hindbrain nuclei and projections influence precerebellar migration.

RESULTS

Dynamic expression of Gli3 in precerebellar progenitors and neurons

Gli3 is expressed in the developing dorsal neural tube and plays important roles in the development of dorsal brain areas (Blaess et al., 2006; Blaess et al., 2008; Haddad-Tóvolli et al., 2012; Hui et al., 1994; Theil et al., 1999; Willaredt et al., 2008). To investigate *Gli3* expression in the developing precerebellar system we performed RNA *in situ* hybridization for *Gli3* and analyzed β-gal expression in *Gli3-lacZ* knock-in mice (*Gli3*$^{lacZ/+}$, Garcia et al., 2010). In the E9.5 hindbrain, *Gli3* was expressed in the entire dorsal area (alar plate),

including the clRL (**Fig. S1A-C** Ray and Dymecki, 2009). By E10.5, *Gli3* was excluded from the dorsal most hindbrain and did no longer overlap with the *Atoh1*-positive MF progenitor domain. The adjacent, *Atoh1*-negative CF domain continued to express *Gli3* (**Fig. S1D-H**). At E9.5 and E10.5, *Gli3* was also expressed in the forming trigeminal ganglia (**Fig. S1A,E**). The *Barhl1* (*BarH like 1)-positive* MF migratory streams and nuclei were negative for *Gli3* at E14.5 and E18.5 (**Fig. S1I-Q**, Li et al., 2004). At these stages, *Gli3* was primarily expressed in the *Er81*-positive subset of the ION (**Fig. S1I,J,O,P,R-W**; Xiang et al., 1996; de Diego et al., 2002; Zhu and Guthrie, 2002; Hashimoto et al., 2012) and in a few non-precerebellar hindbrain structures, including the superior olivary complex, the ventral nucleus of the lateral lemniscus and the solitary nucleus (**Fig. S1X-BB** and data not shown).

Precerebellar nuclei are severely altered in the *Gli3$^{xt/xt}$* hindbrain

To examine whether *Gli3* plays a role in the development of the precerebellar system, we analyzed MF and CF nuclei in mice homozygous for the *Gli3 extratoe (xt)* allele. The *Gli3 xt* allele contains a large deletion that includes the 3' end of the *Gli3* gene, resulting in a loss-of-function phenotype for Gli3. *Gli3$^{xt/xt}$* mice have multiple defects in organ and brain development and die at birth (Hui and Joyner, 1993; Johnson, 1967). At E18.5, the *Barhl1*-expressing PN and RTN were not properly formed in the *Gli3$^{xt/xt}$* hindbrain (**Fig. 1A-F**). *Barhl1*-expressing neurons were located close to the pial surface and were dispersed in discontinous clusters along the ventral midline of r3-r8 in *Gli3$^{xt/xt}$* mutants (**Fig. 1A-N, Fig. S2)**. The distribution of the cells varied in different mutants: in about half of the analyzed brains, cells accumulated at the midline from r3-r8, with most cells positioned in caudal rhombomeres (n=11/20). More than a quarter of the brains (n=7/20) had nuclei of variable size at both the PN/RTN and ION level, with cells sporadically distributed along the rostrocaudal axis. The remaining mutants had no discernible PN/RTN (n=2/20) (**Fig. 1C,D**, **Fig. S2**). The clusters at ectopic caudal positions in *Gli3$^{xt/xt}$* brains were organized similarly to the PN/RTN in controls: cells accumulated at both sites of the ventral midline but were separated by a small gap (coronal sections, n=15/15 at rostral levels, n=11/15 at r6-r8) **Fig. 1C,F**; **Fig. S2F-H,J-L**). *Barhl1*-expressing cells in an extramural layer in the lateral hindbrain at r4-r6 levels of some *Gli3$^{xt/xt}$* mutants were likely remnants of the AES (**Fig. 1F, Fig. S2G**).

At the level of r7/8, *Barhl1*-positive cells clustered where the LRN normally forms, but the presumptive LRN was reduced in size in the *Gli3$^{xt/xt}$* hindbrain and some *Barhl1*-positive cells remained extramurally (**Fig. 1J,N**). *Barhl1* and *Er81* double positive ECN-cells did not cluster dorsally but were dispersed along the dorsolateral pial surface in the *Gli3$^{xt/xt}$* hindbrain (**Fig. 1G-N**). Monitoring the location of labeled cells derived from *Atoh1 (Atonal homolog 1)*-expressing MF progenitors in *Atoh1-Cre, Gli3$^{xt/+}$* and *Atoh1-Cre, Gli3$^{xt/xt}$* mice that also

contained a *Rosa* reporter allele (*R26*$^{lacZ/+}$ or *R26*$^{EYFP/+}$) confirmed the altered distibution of MFN in *Gli3*$^{xt/xt}$ mutants (**Fig. 1O,P; Fig. S2M,N**).

To examine whether clusters of *Barhl1*-positive cells located along the ventral midline of r4-8 were PN/RTN neurons, we analyzed the expression of *Lhx2* (*LIM Homeobox Protein 2*), *Brn3.2* and *Barhl2* (**Fig. 1Q,S,U,W),** three genes that are not expressed in ECN/LRN neurons at E18.5 (data not shown, Mo et al., 2004). *Barhl1*-positive ventral clusters in r7/8 of the *Gli3*$^{xt/xt}$ hindbrain expressed *Lhx2, Brn3.2* and *Barhl2*, confirming their PN identity (**Fig. 1Z,BB,DD,FF**). *Brn3.2* and *Barhl2* are weakly expressed in RTN neurons (**Fig. 1U,W**). Interestingly, *Barhl1*-positive clusters in r4 of *Gli3*$^{xt/xt}$ hindbrains expressed only low levels of *Brn3.2* and *Barhl2*, suggesting that they have an RTN-identity (**Fig. 1V,X**).

Analysis of the expression of the transcription factors *Er81* and FOXP2 (forkhead box P2, labels all ION neurons, Fujita and Sugihara, 2012; Zhu and Guthrie, 2002) showed that the ION was decreased in size and that the rostral ION in r7 was not established in E18.5 *Gli3*$^{xt/xt}$ hindbrains compared to controls. The layered organization of the remaining ION was altered in *Gli3*$^{xt/xt}$ mutants (**Fig. S3A-H)**. In contrast to the variations in the clustering of ectopic MFN neurons, the ION phenotype was comparable in all analyzed mutants (n=8/8)

To investigate whether neurons in the altered precerebellar system in the *Gli3*$^{xt/xt}$ are still able to establish connections to the cerebellum, we performed DiI labeling experiments in which DiI crystals were placed into the E18.5 cerebellum **(Fig. S4A-H).** This analysis showed that at least some ectopic MFN in the caudal hindbrain retain their ability to connect to the cerebellum (**Fig. S4F**). In contrast, we did not detect any DiI labeling in the rostrally located MFN clusters or in the ION in the *Gli3*$^{xt/xt}$ brains, suggesting that MF and CF are not properly established (**Fig. S4D,F**). Whether the apparent loss of ION-cerebellum connections is a primary defect in ION/MFN neurons could not be clarified, since it might be a consequence of the malformed cerebellum in *Gli3*$^{xt/xt}$ brains (Blaess et al., 2008).

MF and CF progenitor domains are established in *Gli3*$^{xt/xt}$ brains

In the clRL, the dorsal *Atoh1*-expressing domain contains MF progenitors while the ventral clRL domain gives rise to CF neurons and is divided into *Ngn1* (neurogenin 1), *Ascl1* (achaete-scute complex homolog 1) and *Ptf1a* (Pancreas specific transcription factor 1a) positive subdomains (**Fig. 2A**, Kim et al., 2008; Ray and Dymecki, 2009; Rodriguez and Dymecki, 2000; Storm et al., 2008; Yamada et al., 2007). Since Gli3 plays a role in dorsoventral fate specification in the neural tube (Persson et al., 2002), we analyzed whether the different transcription factors subdomains in the clRL are altered in E10.5 *Gli3*$^{xt/xt}$ embryos, but did not detect an obvious difference in the size and organization of these domains as compared to controls (**Fig. 2B-J,O** and data not shown). Expression of

Lmx1a, a roof plate marker, was also comparable in control and mutant embryos (**Fig. 2K,L**).

WNT1 is a regulator of progenitor proliferation and, depending on the developmental stage and the rostrocaudal hindbrain level, *Wnt1* expression fully or partially overlaps with the MF and CF progenitor domains (Gibson et al., 2010; Rodriguez and Dymecki, 2000; Ulloa and Martí, 2010). Comparison of the *Wnt1*-positive domain in control and mutant hindbrain at E10.5 did not reveal a difference in domain size or in *Wnt1* expression level (**Fig. 2M-O).** The number of proliferating cells in S-Phase (BrdU-positive cells after 1-hour BrdU pulse) in the *Atoh1*- and NGN1-positive progenitor domain at E10.5 was not significantly different between control and mutant (**Fig. 2P**). In summary, MF or CF progenitor domains are established normally in absence of *Gli3* function and changes in progenitor fate or proliferative potential are unlikely to be the underlying cause for the aberrant organization of precerebellar nuclei in *Gli3*$^{xt/xt}$ mutants.

Altered migratory streams in the developing precerebellar system of *Gli3*$^{xt/xt}$ embryos

Since MF and CF progenitor domains are not altered in *Gli3*$^{xt/xt}$ mutant embryos, the aberrant development of precerebellar nuclei is likely caused by alterations in the corresponding migratory streams. We first investigated the IMS by analyzing *Er81*- and *Brn3.2* positive CF neurons (r7/r8, **Fig. S3I-X**). In control brains, the IMS was present at E12.5, reached the ventral midline by E13.5 and gave rise to the typical layered ION structures at E16.5 (**Fig. S3I-P**). In the *Gli3*$^{xt/xt}$ hindbrain, the IMS was barely discernible at E12.5 and the *Brn3.2*/*Er81*-expressing cells reached the ventral midline only at E14.5 **(Fig. S3Q-X**). In contrast to control animals, in which *Er81* positive/*Brn3.2* negative cells at the tip of the IMS were trailed by a population of *Er81* positive */Brn3.2* positive cells at E12.5 and E13.5 (**Fig. S3I-X**), we could only detect an *Er81/Brn3.2* double-positive cell population in *Gli3*$^{xt/x}$ mutants at E13.5 **(Fig. S3Q-X**). In addition to the delayed migration and the altered composition of the IMS in *Gli3*$^{xt/x}$ mutants, the forming ION domain was reduced in size, in particular in r7, and layering was abnormal in the remaining ION **(Fig. S3Q-Y**). Cell death is unlikely to be the primary cause for the reduced size of the ION, since the number of cleaved caspase-3 expressing CFNs was not increased in E14.5 *Gli3*$^{xt/xt}$ embryos as compared to controls (data not shown).

We next assessed the development of the PES in r7/8. In control embryos, the *Barhl1*-positive PES started to form at E12.5, reached the midline by E13.5 and established the LRN and ECN by E16.5 (**Fig. 3A-D;** Kawauchi et al., 2006). In *Gli3*$^{xt/xt}$ mutant embryos, the PES reached the ventral midline only at E14.5 and *Barhl1*-expressing cells persisted extramurally in the E16.5 *Gli3*$^{xt/xt}$ hindbrain (**Fig. 3E-H**). These results imply a delay in cell migration for both the IMS and PES in *Gli3*$^{xt/xt}$ embryos.

The AES could be visualized as a compact, extramural accumulation of *Barhl1*-positive cells in the dorsolateral hindbrain (r4-r6) of E13.5-E16.5 control brains (**Fig. 3I-L;** Geisen et al., 2008). In *Gli3*$^{xt/xt}$ mutant embryos, *Barhl1*-positive cells started to accumulate extramurally in r4-r6 at E14.5 but were more dispersed than in controls. Between E15.5 and E16.5, extramural *Barhl1*-expressing cells reached the ventral midline and accumulated in ectopic caudal positions (**Fig. 3M-P**). Whole-mount immunostaining for BARHL1 on E13.5 and E16.5 *Gli3*$^{xt/xt}$ and control brains confirmed the delayed onset and disorganization of the MFN migratory streams in *Gli3*$^{xt/xt}$ hindbrains (**Fig. 3U-X′,** Nichols and Bruce, 2006; Geisen et al., 2008).

The ectopic position of PN/RTN neurons in r7/8 of the E18.5 *Gli3*$^{xt/xt}$ hindbrain suggests that some AES cells migrate ventrally instead of turning rostrally. To examine this, we analyzed *Barhl2* expression since it is only expressed in AES, but not PES neurons (**Fig. 3C,J,Q,S**). In *Gli3*$^{xt/xt}$ mutants, *Barhl2* was weakly expressed in the *Barhl1*-positive area in r4-r6 and extended towards the ventral-lateral hindbrain in r7/8 (**Fig. 3G,N,R,T**). These data suggest that a subset of AES cells fails to turn rostrally and instead continues on a ventral path in *Gli3*$^{xt/xt}$ mutants, leading to ectopic accumulation of PN/RTN neurons at the ventral midline of the caudal hindbrain.

The r7/r8 derived-AES subset fails to turn rostrally in *Gli3*$^{xt/xt}$ brains

We next investigated whether a specific subset of AES cells fails to turn rostrally in *Gli3*$^{xt/xt}$ embryos. AES and PN can be topographically divided into three subsets based on a Hox code that reflects the origin of the cells in r6, r7 or r8 (Di Meglio et al., 2013, schematic in **Fig. 4**). To examine how the organization of the AES and of the PN/RTN are affected in *Gli3*$^{xt/xt}$ hindbrain, we analyzed *Hoxb3, Hoxb4*, *Hoxb5* expression at E14.5 and E18.5 and *Lhx2* expression at E14.5. At E14.5, *Lhx2* is most strongly expressed in the *Hoxb3* only population in the AES and in contrast to the Hox genes, it is absent from the PES (**Fig. 4A-B,K,L; Fig. S5**). In E14.5 *Gli3*$^{xt/xt}$ mutants, both *Lhx2* and *Hoxb3* were present in the dispersed AES in r5/r6, while *Hoxb4* and *Hoxb5* were not expressed (**Fig. 4F-J, Fig. S5**). In contrast, in r7/8, where the nascent AES extends ectopically into the ventral hindbrain in the mutant embryos (compare with **Fig. 3G,R),** *Hoxb3, Hoxb4* and *Hoxb5* were present. Weak *Lhx2* was also detected in few AES cells (**Fig. 4P-T′, Fig. S5**). At E18.5, the PN in r4-r6 was negative for *Hoxb4/5* in the mutant hindbrain (**Fig. S6E-H**), while the ectopic PN neurons in r7/8 expressed all three *Hox* genes (**Fig. S6M-P**). *Hoxb3* was expressed broadly in the ectopic PN at this level, while *Hoxb4* and *Hoxb5* were expressed in subdomains, resembling the Hox expression pattern in the PN of controls (**Fig. S6A-D,M-P**). In summary, these data suggest that the AES is split in *Gli3*$^{xt/xt}$ mutants: the r6-derived part (*Hoxb3*/*Lhx2*-positive)

partially retains its ability to migrate rostrally, while the r7/8 derived part (*Hoxb3*/*Hoxb4* or *Hoxb3*/*Hoxb4*/*Hoxb5*-positive) follows a direct route towards the ventral midline (**Fig. 4U**).

Expression of guidance molecules and their receptors is maintained in *Gli3$^{xt/xt}$* hindbrain

Interfering with the function of guidance factors such as SLITs (SLIT1-3), Netrin and the chemokine CXCL12 or their receptors leads to aberrant migration of precerebellar neurons, resulting in phenotypes that appear similar to the ones observed in *Gli3$^{xt/xt}$* mutants (Di Meglio et al., 2008; Dominici et al., 2018; Geisen et al., 2008; Gilthorpe et al., 2002; Kim and Ackerman, 2011; Kuwako et al., 2010; Marillat et al., 2004; Moreno-Bravo et al., 2018; Zhu et al., 2009). Since the SLIT receptors ROBO1/2 have recently been shown to function non-cell autonomously in precerebellar migration (Dominici et al., 2018), we focused our analysis on the expression of *Netrin* and *Cxcl12* and their respective receptors between E13.5 and E15.5 (**Fig. 5, Fig. 8** and data not shown). Expression of *Netrin* in the floor plate and the ventricular neuroepithelium (E13.5-E14.5), and of its receptors *Unc5c* (only expressed in the PES at E13.5 and E14.5) (**Fig. 5A-D,E-H** and data not shown) and DCC (in AES and PES, E14.5-E15.5) was not altered in the Gli3$^{xt/xt}$ hindbrain (**Fig. 8I-P** and data not shown). The Netrin receptor *Unc5b* is restricted to the dorsal AES (Di Meglio et al., 2013). In our hands, *Unc5b* expression was weak even in the compact AES in controls, making it difficult to determine whether *Unc5b* was expressed in the dispersed migratory stream in Gli3$^{xt/xt}$ mutants (data not shown).

ROBO3 forms a complex with DCC, which has been shown to promote ventral migration of precerebellar neurons (Di Meglio et al., 2008; Marillat et al., 2004; Zelina et al., 2014). *Robo3* was prominently expressed in the AES of control and *Gli3$^{xt/xt}$* mutants between E14.5 and E16.5 and in the AES and PES at E13.5 (**Fig. 5I-L, Fig. S7** and data not shown). In IMS cells, *Robo3* is presumably downregulated after their leading processes cross the midline (Di Meglio et al., 2008; Marillat et al., 2004). Indeed, we could not detect *Robo3* expression in the forming ION of control or *Gli3$^{xt/xt}$* embryos at E13.5 and subsequent stages (**Fig. 5K,L, Figure S7** and data not shown), suggesting that midline crossing of ION projections is not affected in *Gli3$^{xt/xt}$* mutant embryos.

The CXCL12 receptor *Cxcr4* was expressed in the AES in E14.5 control brains. In *Gli3$^{xt/xt}$* mutants, *Cxcr4* was only expressed in the AES in r7/8, but was downregulated in the rostrally-migrating AES cells (**Fig. 5M-P**), suggesting that the rostral migration of the AES is independent of *Cxcr4* in absence of *Gli3*. Since inactivation of *Cxcr4* results in disrupted marginal migration (Zhu et al., 2009), the reduced *Cxcr4* expression in the AES may explain the partial delamination of AES neurons into the intramural space observed at E16.5 and E18.5 (compare with **Fig. S2F-H**). The ligand *Cxcl12* was expressed in the meninges and in

the ventral cochlear nucleus in control and *Gli3*$^{xt/xt}$ mutant brains at E15.5 (**Fig. 5Q,R,** Zhu et al., 2009). In summary, these data indicate that alterations in the expression of guidance cues and receptors known to regulate precerebellar migration are unlikely to be the primary cause for the altered migratory streams in *Gli3*$^{xt/xt}$ mutant brains.

Gli3 functions non-cell autonomously in the regulation of mossy fiber neuron migration

Gli3 is only expressed in MF progenitors in the clRL before E10.5 and is not present in the AES or PES (**Fig. S1**), suggesting that *Gli3* regulates migration of MFNs non-cell-autonomously. To investigate this, we inactivated *Gli3* specifically in cells that express *Atoh1* (**Fig. 6A**). In this mouse model (*Atoh1-Gli3* cko, genotype *Atoh1-Cre, Gli3*$^{xt/flox}$), Cre-mediated recombination and thus inactivation of *Gli3* occurs specifically in MF and other RL progenitors around E10.5 (**Fig. 6B-E, K, Fig. S8**). In *Atoh1*-Gli3 cko brains, the location and size of MF nuclei at E18.5 and the organization of the AES and PES at E14.5 was comparable to controls. Moreover, both streams maintained their proper topographical organization as assessed by Hox gene expression (**Fig. 6E-Z**). In summary, these data support a non-cell autonomous role of *Gli3* in MFN migration.

Normal development of precerebellar nuclei when *Gli3* is inactivated in the CNS after E10.5

Based on the continuous expression of *Gli3* in a subdomain of the ION throughout embryonic development, *Gli3* might have a cell-autonomous role in the assembly of the ION (**Fig. S1**). To examine this possibility, we generated a CNS specific *Gli3* conditional knock-out using *Nestin-Cre* (termed *Nes-Gli3* cko; **Fig. 7A**). In this mouse model, recombination in the CNS, including the entire hindbrain, starts around E10 (**Fig. 7B,** Blaess et al., 2006; Graus-Porta et al., 2001). We did not detect any phenotypes in MF or CF streams or nuclei in these mutants at E14.5 or E18.5 (**Fig. 7C-J, Fig. S9** and data not shown). These results demonstrate that (1) the normal development of the ION does not depend on Gli3 function after E10.5 and (2) that the overall development of the precerebellar system is not affected by inactivation of *Gli3* in the CNS after E10.5.

Organization of non-precerebellar hindbrain nuclei is not obviously altered in the *Gli3*$^{xt/xt}$ hindbrain

Since the conditional gene inactivation of *Gli3* suggests a non-cell autonomous role of Gli3 in precerebellar migration, we investigated whether defective precerebellar development might be a consequence of overall altered hindbrain development. It has previously been suggested that specific cell clusters, such as the facial motor nucleus, may act as

guideposts for the AES (Geisen et al. 2008). Analysis of *Isl1* (*Islet 1*) expression showed that the hindbrain motor nuclei, including the facial motor nucleus, were properly established in the *Gli3*$^{xt/xt}$ hindbrain at E14.5 (**Fig. S10A** and data not shown). The principal trigeminal nucleus (Pr5) and spinal trigeminal nucleus (Sp5) are derived from the dorsal, *Gli3*-expressing hindbrain neuroepithelium and *Atoh1*-expressing RL. These nuclei, which are located along the migratory pathway of the AES or the AES and PES, respectively, are *Lhx2, Lhx9*, *Pax2*-positive (Pr5) or *Lhx2*/*Lhx9*/*Pax2*/*Gbx2*-positive (caudal Sp5). The oral Sp5 is only *Lhx2*-positive. Based on these markers, the Pr5 and the caudal and oral Sp5 were established in *Gli3*$^{xt/xt}$ embryos (**Fig. S10B-E** and data not shown). The *Pax2*-positive median raphe nucleus and the *Gbx2*-positive gigantocellular reticular nucleus were analyzed as examples of ventrally derived nuclei and these were also formed in *Gli3*$^{xt/xt}$ hindbrain (**Fig. S10D,E** and data not shown). To assess whether Gli3 might play a general role in development of lRL derived-neurons, we analyzed the cochlear extramural stream (*Robo3*/*Lmx1a* positive, *Barhl2* negative) and ventral cochlear nuclei (*MafB* positive), which are generated in the rostral lRL in r2-r5, in control and *Gli3*$^{xt/xt}$ embryos. We found that these RL derived-structures were formed in *Gli3*$^{xt/xt}$ embryos (**Fig. S10F-J** and data not shown). Thus, severe defects in hindbrain development appeared to be restricted to clRL-derivatives in the *Gli3*$^{xt/xt}$ mutants. While we cannot fully exclude that there are subtle changes in other non-precerebellar hindbrain nuclei and their projections, these results suggest that alterations in non-precerebellar hindbrain nuclei may not be the primary cause of the precerebellar defects.

The trigeminal spinal tract is disrupted in *Gli3*$^{xt/xt}$ mutants

AES neurons pass the roots of cranial nerves during their rostral-ventral directed movement (Nichols and Bruce, 2006, Kratchowil et al. 2017) and AES and ION neurons have been shown to migrate along cranial nerve roots to the periphery in absence of interactions with their preferred guidance cue Netrin in the pial surface (Mehlen et al. 2018, Yung et al.2018). This prompted us to examine whether alterations in cranial ganglia and their projections may contribute to the defects in the precerebellar system of *Gli3*$^{xt/xt}$ embryos. Using ISL1 immunostaining, we found that the trigeminal ganglia were expanded caudally in E14.5 *Gli3*$^{xt/xt}$ mutants and that cell death (cleaved caspase-3 positive cells) was significantly reduced in *Gli3*$^{xt/xt}$ trigeminal ganglia as compared to controls (**Fig. 8A-H).** The size of other cranial ganglia was not obviously altered in *Gli3*$^{xt/xt}$ mutants (data not shown). DiI labeling of the trigeminal ganglia at E14.5 and whole-mount immunostaining of E18.5 brains for peripherin (PRPH), an intermediate filament that is primarily expressed in neurons of the peripheral nervous system, showed that the central descending sensory tract of the trigeminal ganglion, the trigeminal spinal tract (sp5) was highly disorganized in *Gli3*$^{xt/xt}$

mutants (**Fig. S11**), suggesting that loss of *Gli3* function affects the development of the trigeminal ganglia and its central projections.

Rostrally-migrating precerebellar neurons are in close apposition to the trigeminal spinal tract in the wild-type hindbrain

The sp5 terminates in the spinal trigeminal nucleus (Sp5), which extends from the caudal hindbrain into the upper cervical spinal cord. To gain insight whether the sp5 could potentially serve as a guidance structure for migrating precerebellar neurons, we performed immunostaining for PRPH to label cranial tracts and for DCC to label MFNs in E14.5 *Gli3*$^{xt/xt}$ and control embryos (**Fig. 8-Q**). In controls, the forming AES was located dorsally to the sp5 in its initial migration phase in r7/8 (**Fig. 8O**). During its rostrally-oriented migration, the AES was positioned just lateral to the sp5 and cells in the ventral AES were in close contact with the tract (**Fig. 8K,M; Movie S1**). In r3/4, where the AES turns ventrally to reach the ventral midline, the AES was again separated from the sp5 (**Fig. 8I**). In *Gli3*$^{xt/xt}$ mutants, analysis of the PRPH immunostaining confirmed that the sp5 was disorganized and less fasciculated than in controls. DCC immunostaining revealed that the AES was fragmented into small clusters in *Gli3*$^{xt/xt}$ mutants, as previously shown with *Barhl1* in situ hybridization (compare with **Figure 4F-H**) and that the AES was largely detached from the sp5 in the mutant embryos (**Figure 8L,N,P**). These data show that AES neurons normally migrate in close apposition to the sp5 during their rostrally-oriented movement and that the loss of *Gli3* results in the defasciculation of sp5 and an apparent detachment of AES neurons from the tract. Together these results suggest that the disorganization of the sp5 might be one factor contributing to the defects in AES migration in *Gli3*$^{xt/xt}$ embryos.

DISCUSSION

Gli3 and patterning of the hindbrain

Gli3 regulates early patterning events in spinal cord, cortex, dorsal midbrain and cerebellum (Blaess et al., 2008; Persson et al., 2002; Theil et al., 1999). In the *Gli3*$^{xt/xt}$ spinal cord, progenitor domains at intermediate levels of the dorsoventral axis (known as p1 and dl6), which express *Nkx6-2, Dbx1 or Dbx2*, are expanded dorsally as compared to controls. In contrast, more dorsal progenitor domains (known as dl5 and dl4) are decreased in size (Persson et al., 2002). In the *Gli3*$^{xt/xt}$ hindbrain, only a *Nkx6-1*-expressing domain is expanded and only in r1-r3 (Lebel et al., 2007). Alterations in the most dorsal domains (dl1-dl3 in spinal cord, RL in hindbrain) have not yet been described in *Gli3*$^{xt/xt}$ mutants. We show that the size of clRL domains are not changed in *Gli3*$^{xt/xt}$ mutants and that *Gli3* expression is downregulated in the most dorsal part of the clRL domain after E9.5. Moreover, we could not

detect any severe alterations in the organization of non-precerebellar caudal hindbrain nuclei in *Gli3*$^{xt/xt}$ mutants. Even the lRL-derived cochlear nucleus was established correctly in the mutants. Based on these data and a previous analysis of the *Gli3*$^{xt/xt}$ hindbrain (Lebel et al., 2007) we propose that indirect effects of patterning defects in the caudal hindbrain of *Gli3*$^{xt/xt}$ mutants are not the most likely explanation for the alterations in precerebellar development. Nevertheless, we cannot exclude that our analysis missed more subtle defects in the organization of hindbrain nuclei or alterations in their projections in the *Gli3*$^{xt/xt}$ brain, which might be of consequence for the migration of precerebellar neurons. Finally, as recently proposed by Dominici et al (Dominici et al., 2018), severe developmental defects, such as the ones occurring in *Gli3* null mutants, might have unspecific consequences on neuronal development, including the development of the hindbrain precerebellar system.

Indirect effects on precerebellar migration

Using conditional gene inactivation, we demonstrate that Gli3 is unlikely to have a cell-autonomous role in the migration of MFNs. This result is consistent with the observation that *Gli3* is largely excluded from the MF progenitor domain after E9.5 and is not expressed in migrating MFNs. Notably, recent data show that even guidance factors that are important regulators of precerebellar migration do not act directly on the migrating neurons (Dominici et al., 2018). In null mutants for the guidance factors *Slit1/2* or for the Slit receptors *Robo1/2* the AES is not well defined, *Barhl1*-positive cells accumulate in ectopic positions at the ventral midline in r4-r8 and the ION is abnormally formed (Di Meglio et al., 2008; Dominici et al., 2018; Geisen et al., 2008), a phenotype closely resembling the one in *Gli3* null mutants. However, specific inactivation of *Robo1/2* in precerebellar progenitors does not affect precerebellar migration and nuclei formation. Inactivation of *Slit1/2* in the floor plate and in the facial motor nucleus, structures postulated to be important sources of SLITs for migrating precerebellar neurons, results in only a mild phenotype (Dominici et al., 2018). Thus, it is currently unclear, which primary defect in *Slit/Robo* null mutants leads to aberrant precerebellar migration.

Two recent studies show that Netrin 1 is not just expressed in the hindbrain floor plate, but is also secreted at the basal lamina by neural progenitor endfeet. Inactivation of Netrin results in subsets of AES and IMS cells moving ectopically from the CNS into the PNS (Moreno-Bravo et al., 2018; Yung et al., 2018). In *Gli3*$^{xt/xt}$ mutants, precerebellar neurons stay within the CNS, indicating that Netrin-mediated guidance is not affected. The fact that precerebellar neurons migrate along cranial nerve roots in absence of Netrin, suggests however that projections from the cranial ganglia may, in principle, serve as corridors for precerebellar migration.

The spinal trigeminal tract and precerebellar migration

Based on our results, rostrally-migrating AES neurons might interact with the sp5 during this phase of their migration. Thus, the altered development of the trigeminal ganglia and its descending central sensory tract, sp5, might contribute to the altered migration of AES neurons in *Gli3*$^{xt/xt}$ mutants by disrupting this potential interaction. Central axons of the trigeminal ganglia appear as early as E12.5 in rat, ascending and descending branches are established at E13.5 and the descending branches, which form the sp5, reach the caudal hindbrain one day later (Miyahara et al., 2003). Thus, the sp5 is already established by the time the AES starts to form and ideally positioned to function as a tract for rostrally-migrating AES neurons.

We show that AES neurons cluster in close apposition to the sp5 during their rostral migration. Cells in the ventral part of the AES, corresponding to the Hoxb3/4/5-expressing AES cells, appear to be in direct contact with the sp5. In *Gli3* null mutants, the ventral *Hoxb3/4/5*-expressing AES cells fail to switch from a ventrally-oriented migration to a rostrally-oriented migration and the AES appears to be detached from a defasciculated sp5. An influence of the sp5 on IMS or PES migratory streams, which are also altered in *Gli3*$^{xt/xt}$ mutant mice, is less evident. Instead, the defects in the LRN/ECN formation could be a consequence of the accumulation of ectopic PN/RTN cells in the caudal hindbrain in *Gli3*$^{xt/xt}$ mutant embryos, while the changes in the IMS and ION might be primarily related to a reduction in their cell number.

Role of Gli3 in the development of the cranial sensory system

Cranial ganglia including the trigeminal ganglia are derived from both ectodermal placodes and cranial neural crest (Steventon et al., 2014). The disorganization of the sp5 might be linked to a caudal expansion of the trigeminal ganglia in *Gli3* null mutants. An increased size in cranial sensory ganglia has already been noted in the original description of the *extratoe* phenotype (Johnson, 1967). Highly-elevated Shh signaling leads to severely altered development of trigeminal and facial nerves. This effect may be mediated through the negative regulation of Wnt signaling by Shh (Kurosaka et al., 2015). Whether the loss of Gli3 and its effect on cranial nerve organization might also be caused by altered Wnt signaling remains to be investigated, but data from the spinal cord demonstrate that Gli3 inhibitory activity negatively regulates the canonical Wnt signaling pathway by interacting with β-catenin (Ulloa et al., 2007).

Conclusion

In summary, we identify a previously uncharacterized function of the zinc finger transcription factor Gli3 in regulating precerebellar migration and trigeminal ganglia development. We also show that Gli3 likely acts in an indirect manner on precerebellar migration. Together with the recently published studies that revise the role of Netrin and Slit/Robo in precerebellar migration (Dominici et al., 2018; Moreno-Bravo et al., 2018; Yung et al., 2018) our results imply that the regulation of precerebellar migration is even more intricate than anticipated. We propose that in order to fully unravel the mechanisms that guide these migratory streams in the hindbrain, it will be necessary to consider hindbrain fiber tracts as a potential source for guidance cues or as a substrate for migrating precerebellar neurons.

MATERIALS AND METHODS

Mouse lines

Mice were housed at a maximum of five animals per cage with a standard 12-h light/dark cycle and given food and water *ad libitum*. Experiments were performed in compliance with the guidelines for the welfare of animals issued by the Federal Government of Germany and the directives of the European Union. *Gli3*^{Xt} (Hui and Joyner, 1993), *Gli3*^{flox} (Blaess et al., 2008), *Gli3*^{lacZ} (Garcia et al., 2010), *Nestin-Cre* (Tronche et al., 1999), *Atoh1-Cre* (Matei et al., 2005), *Rosa26-stop-lox-stop lacZ* (*R26*$^{lacZ/+}$, Soriano, 1999) and *Rosa26-stop-lox-stop EYFP* (*R26*$^{EYFP/+}$, Srinivas et al., 2001) were genotyped as described. Noon of the day of the vaginal plug was assigned as embryonic day 0.5 (E0.5). The following conditional knock-out (cko) mice were generated: *Nes-Gli3* cko (*Nestin-Cre, Gli3*$^{xt/flox}$) and *Atoh1-Gli3* cko (*Atoh1-Cre, Gli3*$^{xt/flox}$). We have previously established that mice homozygous for the *Gli3*^{Xt} allele (*Gli3*$^{Xt/Xt}$) and mice homozygous for the recombined floxed allele (*Gli3*$^{rec/rec}$) display comparable brain phenotypes, indicating that both alleles are *Gli3* null alleles (Blaess et al., 2008). A few *Gli3*$^{xt/xt}$ mutants displayed exencephaly, these mutants were excluded from the analysis.

BrdU injections

For BrdU (Bromdesoxyuridin; Merck, Darmstadt, Germany) labeling of embryos, pregnant dams were injected intraperitoneally with 100 µg BrdU/g body weight and sacrificed 1 h later.

Immunofluorescence and X-gal analysis

Embryos or embryonic brains were dissected, collected in cold 0.1M phosphate-buffered saline (PBS), and embryonic tail samples were collected separately for DNA extraction and

genotyping. The embryos were fixed overnight at 4°C in 4% paraformaldehyde (PFA) in 0.1M PBS. After rinsing twice in 0.1M PBS for 30 min the embryos were either treated in an ascending sucrose series (15 and 30% in 0.1M PBS) and mounted in Tissue Tek freezing medium (Sakura, Turrance, USA) or dehydrated and processed for paraffin embedding. X-gal staining of 14 µm cryosections and immunostaining of 14 µm cryosections or 7 µm paraffin sections were performed as described (Blaess et al., 2011). Following primary antibodies, all of which have been validated in previous publications, were used: mouse anti-BrdU (3D4; BD Biosciences; Lot: 25098, Sudarov et al., 2011) 1:50; mouse anti-cleaved caspase 3 (5AE1, Cell Signaling Technologies, Blaess et al. 2006 & antibody validation on provider's website) 1:200; goat anti-DCC (A-20, sc-6535 Santa Cruz Biotechnology, Lot:L1610; Dominici et al. 2018) 1:400,goat anti-FOXP2 (S262, Cat. No. EB05226, Everest Biotech, Lot: S2G2; Fujita and Sugihara, 2012) 1:200; rat anti-GFP (Cat.-No., 04404-84; Nacalai Tesque; Lot: M8A3283, Sudarov et al., 2011); rabbit anti-GFP (A11122, Life Technologies, Lot:1828014&178991; Sudarov et al., 2011); mouse anti-ISL1 (39.3F7, DSHB; Roy et al., 2012) 1:50; goat anti-NGN1 (A-20, sc-19231, Santa Cruz Biotechnology, Lot: A1209; Di Giovannantonio et al., 2014) 1:200; rabbit anti-PRPH (AB1530, EMD Millipore, Lot:2972430; Ter-Avetisyan et al., 2018) 1:200. The following secondary antibodies were used: Cy3-conjugated donkey anti-rabbit, anti-mouse or anti-goat (Jackson Immuno Research Laboratories) 1:200; Alexa 488-conjugated donkey anti-rabbit or anti-mouse IgG (Thermo Fischer Scientific, Waltham, USA) 1:500, Alexa 488-conjugated goat anti-rabbit, anti-mouse, Alexa 546-conjugated goat anti rabbit or anti-guinea pig (Thermo Fischer Scientific) 1:1000. For immunofluorescent detection of transcription factors, sections were treated with 1 mM EDTA at 65°C for 10 min and incubated with biotinylated anti-mouse or anti-goat secondary antibodies (Jackson Immuno Research Laboratories) 1:200, followed by Cy3-conjugated Streptavidin (Jackson Immuno Research Laboratories) 1:1000. For BrdU immunostaining, the sections were fixed in 4% PFA for 10 minutes at room temperature, treated with 2N HCL for 30 minutes at 37 °C and quickly rinsed in boric acid buffer, followed by a standard immunostaining protocol (Blaess et al., 2011).

In situ hybridization

RNA *in situ* hybridization was essentially performed as previously described (Blaess et al., 2011). Frozen sections were fixed in 4% PFA and washed in PBS. Paraffin sections were deparaffinized, rehydrated, treated with Proteinase K (Roche, Penzberg, Germany) and then acetylated. After washing in H_2O, frozen and paraffin sections were dehydrated in different concentrations of ethanol (70%, 80%, 95% and 100%) and incubated in chloroform to de-fat the sections. After hybridization with the cRNA probes and immunodetection of digoxigenin with alkaline phosphatase conjugated antibody (Roche, Penzberg, Germany), sections were

incubated with BM purple (Roche, Penzberg, Germany). The color reaction was stopped in Tris-EDTA buffer. Following *in situ* probes were used: *Ascl1* (Sudarov et al., 2011)*; Atoh1* (Corrales et al., 2004)*; Barhl1* (Bulfone et al., 2000), IMAGE clone ID 335997, accession number W36375); *Barhl2* (Saba et al., 2003) Tetsuichiro Saito); *Brn3.2* (Karagogeos and Wassef, 2002); *Cxcl12* and *Cxcr4* (Tissir et al., 2004); *Er81; Gli3* (Corrales et al., 2004)*; Hoxb3, Hoxb4* and *Hoxb5* (Rob Krumlauf); *Isl1* (Blaess et al., 2008)*; Lhx2* (Rétaux et al., 1999); *Lmx1a* (Blaess et al., 2011); *Netrin1* (Hammond et al., 2009); *Ngn1* (Liu et al., 2008), Mengshen Qiu); *Pax2* (Asano and Gruss, 1992)*; Ptf1a (*bp 1023-1490 of cDNA*); Robo1* and *Robo2* (Bagri et al., 2002), *Robo3* (Marillat et al., 2004), *Slit1* and *Slit2* (Bagri et al., 2002); *Slit3* (Geisen et al., 2008); *Unc5b* (Lu et al., 2004); *Unc5c* (Przyborski et al., 1998).

Whole mount immunostaining

E13.5, E16.5, and E18.5 brains, were dissected, fixed in 4% PFA overnight at 4C and rinsed three times in PBS. The tissue was then dehydrated, bleached, rehydrated, and immunolabeled as described by (Renier et al., 2014; https://idisco.info/idisco-protocol/update-history/). Brains were incubated with antibodies for 24-48 hrs with rabbit anti-Barhl1 (1:500, HPA004809, Sigma Aldrich, Lot: A114004; Dominici et al. 2018) or rabbit anti-PRPH (1:200, AB1530, EMD Millipore, see above for details) and biotin anti-rabbit (1:200; 711065152, Jackson ImmunoResearch) antibodies. Colorimetric detection was achieved using the HRP Vectastain Elite ABC Kit (PK-6100; Vector Laboratories) and the DAB Peroxidase Substrate (SK-4100; Vector Laboratories).

DiI/DiO axonal tracing: Embryonic brains of control and *Gli3*$^{xt/xt}$ mice were removed from the skull with the trigeminal ganglia attached and were fixed overnight with 4% PFA at 4°C. Brains were rinsed three times in PBS to remove residual PFA. Several small crystals of 1,1´-Dioctadecyl-3,3,3´,3´-tetramethylindocarbocyanine perchlorate (DiI, D282; Molecular Probes) or 3,3´-Dioctadecyloxacarbocyanine perchlorate (DiO, D275; Molecular Probes) were attached to the tip of a glass needle. Crystals were placed medially and laterally on the exposed area of one cerebellar hemisphere to retrogradely label precerebellar inputs or on the trigeminal ganglia to anterogradely label the sp5 tract. In a few embryos, the was used instead of the DiI to label the trigeminal ganglion. The brains were first kept in 1% PFA at 37°C for 4 days and then at room temperature for 1 month in the dark. The brains were washed in PBS, were embedded in 3% Ultra Pure LMP Agarose (15517-022, Life Technologies), and were cut at a thickness of 80 µm with a vibratome. The sections were counterstained with Hoechst, were mounted with Fluoromount (F4680, Sigma Aldrich), and were imaged. To visualize the distribution of the different precerebellar neurons, adjacent

sections were immunostained for Barhl1 (1:500, HPA004809, Sigma Aldrich) or FoxP2 (1:200, EB05226; Everest Biotech).

Image acquisition

Bright field images were acquired with a Leica DM1000 microscope (Leica, Wetzlar, Germany) or an inverted microscope (Axio Observer, Zeiss, Oberkochen, Germany). Images of immunofluorescent samples and DiI/DiO labeled samples were acquired with an inverted fluorescence microscope (Axio Observer, Zeiss) using 10x, 20x, 40x or 63x objectives (EC Plan-Neofluar, Zeiss). Structured illumination (ApoTome, Zeiss) was used to acquire images with the 20x, 40x and 63x objectives. 63x objective images were obtained as maximum intensity projections of Z-stack mosaics. The Zeiss Mosaix software was used to assemble images if more than one image was acquired to cover a region of interest. 3D-projection was assembled in ImageJ.

Determining rhombomere levels in the hindbrain

To define rhombomere levels in the developing hindbrain, morphological features such as the location of the cochlear nuclei, precerebellar nuclei, otic vesicles, various motor nuclei and cranial nerves (Farago et al., 2006; Geisen et al., 2008; Guthrie, 2007; Nichols and Bruce, 2006; Paxinos et al., 2006; Paxinos et al., 2012; Schambra, 2008) were taken into consideration. In addition, rhombomere levels were assessed by analyzing the expression of *Hoxb3*, *Hoxb4* and *Hoxb5* (Philippidou and Dasen, 2013).

Quantification

Progenitor domain: The area of domains positive for progenitor markers were measured in E10.5 hindbrains (n ≥ 3 brains per genotype, in sections of 5 levels for each hindbrain, results of only one level are shown in Fig. 2). The progenitor domain areas were normalized to the area of hindbrain tissue measured at the same level.

ION: The area of domains positive for *Er81* or *Brn3.2* were measured in E15.5 hindbrains (n ≥ 3 brains per genotype, in sections of 7 levels for each hindbrain). The area of the expression domains was normalized to the area of hindbrain tissue measured at the same level.

BrdU positive cells: BrdU positive cells were counted within the progenitor domains expressing *Atoh1* or NGN1 at r6/7. The expression of the two progenitor markers was analyzed on adjacent sections. The number of BrdU positive cells was normalized to the area of the respective progenitor domain (n ≥ 3 brains per genotype, three levels per hindbrain, results of only one level are shown in Fig.2).

Quantification of size and cell death in trigeminal ganglion: At the level of r3-5, ISL1 and cleaved Caspase-3 positive cells were counted (n ≥ 3 brains per genotype). Area size or cell counts are presented for the different levels. For the cleaved Caspase-3 quantification, numbers of cleaved Caspase-3-positive cells and ISL positive cells at the different levels were added up and the number of cleaved Caspase-3 positive cells was normalized to the number of ISL1 positive cells.

Areas were quantified using the ImageJ software package 1.48v (http://rsb.info.nih.gov/ij/).

Statistical analysis

Analysis was done non-blinded, since the mutant phenotype was obvious. There was no randomization in the groups and no statistical method was used to predetermine sample sizes. Statistical analysis of histological data was performed using Student´s t-test, parametric one-way analysis of variance (ANOVA) with a post-hoc Tukey or non-parametric Kurskal-Wallis-Test (Origin 8, Origin lab and Prism7, Graphpad). Levene´s test was used to assess equality of variances. Significance levels were set at $p<0.05$. The values are represented as mean ± SD.

Acknowledgements

ISL1 antibody was obtained through the Developmental Studies Hybridoma Bank under the auspices of the National Institute of Child Health and Human Development and maintained by The University of Iowa (Iowa City, IA). The authors would like to thank Susan Ackerman, Alain Chédotal, Robert Edwards, Anne Eichmann, André Goffinet, Alexandra Joyner, Robb Krumlauf, Mengshen Qiu, Sylvie Rétaux, Filippo Rijli, Tetsuichiro Saito and Marion Wassef for *in situ* probes; Ulrich Schüller for the Atoh1-Cre mice and Martin Jansen for technical support.

Competing interests

The authors declare no competing or financial interests.

Author contribution

E.M.C, C.S., S.B. and A.W. carried out experiments. S.B. and E.M.C. designed experiments, and analyzed data. S.B. and E.M.C wrote the manuscript with contributions from all authors. S.B. designed the study. All authors read and approved the final manuscript.

Funding

The authors were supported by the DFG (BL767-2/1 and BL767-3/1); the North-Rhine-Westphalia Repatriation Program of the Ministry for Science of North Rhine Westphalia; the Maria von Linden-Program, University of Bonn (all to SB), and a DAAD doctoral fellowship (to EMC).

REFERENCES

Asano, M. and Gruss, P. (1992). Pax-5 is expressed at the midbrain-hindbrain boundary during mouse development. *Mech Dev* **39**, 29–39.

Bagri, A., Marín, O., Plump, A. S., Mak, J., Pleasure, S. J., Rubenstein, J. L. R. and Tessier-Lavigne, M. (2002). Slit proteins prevent midline crossing and determine the dorsoventral position of major axonal pathways in the mammalian forebrain. *Neuron* **33**, 233–248.

Blaess, S., Bodea, G. O., Kabanova, A., Chanet, S., Mugniery, E., Derouiche, A., Stephen, D. and Joyner, A. L. (2011). Temporal-spatial changes in Sonic Hedgehog expression and signaling reveal different potentials of ventral mesencephalic progenitors to populate distinct ventral midbrain nuclei. *Neural Dev.* **6**, 29.

Blaess, S., Corrales, J. D. and Joyner, A. L. (2006). Sonic hedgehog regulates Gli activator and repressor functions with spatial and temporal precision in the mid/hindbrain region. *Development* **133**, 1799–1809.

Blaess, S., Stephen, D. and Joyner, A. L. (2008). Gli3 coordinates three-dimensional patterning and growth of the tectum and cerebellum by integrating Shh and Fgf8 signaling. *Development* **135**, 2093–2103.

Bloch-Gallego, E., Causeret, F., Ezan, F., Backer, S. and Hidalgo-Sánchez, M. (2005). Development of precerebellar nuclei: instructive factors and intracellular mediators in neuronal migration, survival and axon pathfinding. *Brain Res. Brain Res. Rev.* **49**, 253–266.

Bulfone, A., Menguzzato, E., Broccoli, V., Marchitiello, A., Gattuso, C., Mariani, M., Consalez, G. G., Martinez, S., Ballabio, A. and Banfi, S. (2000). Barhl1, a gene belonging to a new subfamily of mammalian homeobox genes, is expressed in migrating neurons of the CNS. *Hum. Mol. Genet.* **9**, 1443–1452.

Burgess, R. W. (2006). Motor Axon Guidance of the Mammalian Trochlear and Phrenic Nerves: Dependence on the Netrin Receptor Unc5c and Modifier Loci. *J. Neurosci.***26**, 5756–5766.

Corrales, J. D., Rocco, G. L., Blaess, S., Guo, Q. and Joyner, A. L. (2004). Spatial pattern of sonic hedgehog signaling through Gli genes during cerebellum development. *Development* **131**, 5581–5590.

de Diego, I., Kyriakopoulou, K., Karagogeos, D. and Wassef, M. (2002). Multiple influences on the migration of precerebellar neurons in the caudal medulla. *Development* **129**, 297–306.

Di Giovannantonio, L. G., Di Salvio, M., Omodei, D., Prakash, N., Wurst, W., Pierani, A., Acampora, D. and Simeone, A. (2014). Otx2 cell-autonomously determines dorsal mesencephalon versus cerebellum fate independently of isthmic organizing activity. *Development* **141**, 377–388.

Di Meglio, T., Kratochwil, C. F., Vilain, N., Loche, A., Vitobello, A., Yonehara, K., Hrycaj, S. M., Roska, B., Peters, A. H. F. M., Eichmann, A., et al. (2013). Ezh2

orchestrates topographic migration and connectivity of mouse precerebellar neurons. *Science* **339**, 204–207.

Di Meglio, T., Nguyen-Ba-Charvet, K. T., Tessier-Lavigne, M., Sotelo, C. and Chédotal, A. (2008). Molecular mechanisms controlling midline crossing by precerebellar neurons. *J. Neurosci.* **28**, 6285–6294.

Dominici, C., Rappeneau, Q., Zelina, P., Fouquet, S. and Chédotal, A. (2018). Non-cell autonomous control of precerebellar neuron migration by Slit and Robo proteins. *Development* **145**, dev150375

Englund, C., Kowalczyk, T., Daza, R. A. M., Dagan, A., Lau, C., Rose, M. F. and Hevner, R. F. (2006). Unipolar brush cells of the cerebellum are produced in the rhombic lip and migrate through developing white matter. *J. Neurosci.* **26**, 9184–9195.

Farago, A. F., Awatramani, R. B. and Dymecki, S. M. (2006). Assembly of the brainstem cochlear nuclear complex is revealed by intersectional and subtractive genetic fate maps. *Neuron* **50**, 205–218.

Fujita, H. and Sugihara, I. (2012). FoxP2 expression in the cerebellum and inferior olive: Development of the transverse stripe-shaped expression pattern in the mouse cerebellar cortex. *J. Comp. Neurol.* **520**, 656–677.

Garcia, A. D. R., Petrova, R., Eng, L. and Joyner, A. L. (2010). Sonic hedgehog regulates discrete populations of astrocytes in the adult mouse forebrain. *J. Neurosci.* **30**, 13597–13608.

Geisen, M. J., Di Meglio, T., Pasqualetti, M., Ducret, S., Brunet, J.-F., Chédotal, A. and Rijli, F. M. (2008). Hox paralog group 2 genes control the migration of mouse pontine neurons through slit-robo signaling. *Plos Biol*. **6**, e142.

Gibson, P., Tong, Y., Robinson, G., Thompson, M. C., Currle, D. S., Eden, C., Kranenburg, T. A., Hogg, T., Poppleton, H., Martin, J., et al. (2010). Subtypes of medulloblastoma have distinct developmental origins. *Nature* **468**, 1095-1099.

Gilthorpe, J. D., Papantoniou, E.-K., Chédotal, A., Lumsden, A. and Wingate, R. J. T. (2002). The migration of cerebellar rhombic lip derivatives. *Development* **129**, 4719–4728.

Graus-Porta, D., Blaess, S., Senften, M., Littlewood-Evans, A., Damsky, C., Huang, Z., Orban, P., Klein, R., Schittny, J. C. and Müller, U. (2001). Beta1-class integrins regulate the development of laminae and folia in the cerebral and cerebellar cortex. *Neuron* **31**, 367–379.

Guthrie, S. (2007). Patterning and axon guidance of cranial motor neurons. *Nat. Rev. Neurosci.* **8**, 859–871.

Haddad-Tóvolli, R., Heide, M., Zhou, X., Blaess, S. and Alvarez-Bolado, G. (2012). Mouse thalamic differentiation: gli-dependent pattern and gli-independent prepattern. *Front. Neurosci.* **6**, 27–27.

Hammond, R., Blaess, S. and Abeliovich, A. (2009). Sonic hedgehog is a chemoattractant for midbrain dopaminergic axons. *PLoS ONE* **4**, e7007.

Hashimoto, M., Ito, R., Kitamura, N., Namba, K. and Hisano, Y. (2012). Epha4 controls the midline crossing and contralateral axonal projections of inferior olive neurons. *J. Comp. Neurol.* **520**, 1702–1720.

Hui, C. C. and Joyner, A. L. (1993). A mouse model of greig cephalopolysyndactyly syndrome: the extra-toesJ mutation contains an intragenic deletion of the Gli3 gene. *Nat. Genet.* **3**, 241–246.

Hui, C. C., Slusarski, D., Platt, K. A., Holmgren, R. and Joyner, A. L. (1994). Expression of three mouse homologs of the Drosophila segment polarity gene cubitus interruptus, Gli, Gli-2, and Gli-3, in ectoderm- and mesoderm-derived tissues suggests multiple roles during postimplantation development. *Dev. Biol.* **162**, 402–413.

Johnson, D. R. (1967). Extra-toes: a new mutant gene causing multiple abnormalities in the mouse . *J. Embryol. Exp. Morph.* **17**, 543–548.

Kawauchi, D., Taniguchi, H., Watanabe, H., Saito, T. and Murakami, F. (2006). Direct visualization of nucleogenesis by precerebellar neurons: involvement of ventricle-directed, radial fibre-associated migration. *Development* **133**, 1113–1123.

Kim, D. and Ackerman, S. L. (2011). The UNC5C netrin receptor regulates dorsal guidance of mouse hindbrain axons. *J. Neurosci.***31**, 2167–2179.

Kim, E. J., Battiste, J., Nakagawa, Y. and Johnson, J. E. (2008). Ascl1 (Mash1) lineage cells contribute to discrete cell populations in CNS architecture. *Mol. Cell Neurosci.* **38**, 595–606.

Kratochwil, C. F., Maheshwari, U. and Rijli, F. M. (2017). The Long Journey of Pontine Nuclei Neurons: From Rhombic Lip to Cortico-Ponto-Cerebellar Circuitry. *Front. Neural Circuits* **11**, 552–19.

Kurosaka, H., Trainor, P. A., Leroux-Berger, M. and Iulianella, A. (2015). Cranial nerve development requires co-ordinated Shh and canonical Wnt signaling. *PLoS ONE* **10**, e0120821.

Kuwako, K.-I., Kakumoto, K., Imai, T., Igarashi, M., Hamakubo, T., Sakakibara, S.-I., Tessier-Lavigne, M., Okano, H. J. and Okano, H. (2010). Neural RNA-Binding Protein Musashi1 Controls Midline Crossing of Precerebellar Neurons through Posttranscriptional Regulation of Robo3/Rig-1 Expression. *Neuron* **67**, 407–421.

Lebel, M., Mo, R., Shimamura, K. and Hui, C.-C. (2007). Gli2 and Gli3 play distinct roles in the dorsoventral patterning of the mouse hindbrain. *Dev. Biol.* **302**, 345–355.

Li, S., Qiu, F., Xu, A., Price, S. M. and Xiang, M. (2004). Barhl1 regulates migration and survival of cerebellar granule cells by controlling expression of the neurotrophin-3 gene. *J. Neurosci.* **24**, 3104–3114.

Liu, Z., Li, H., Hu, X., Yu, L., Liu, H., Han, R., Colella, R., Mower, G. D., Chen, Y. and Qiu, M. (2008). Control of precerebellar neuron development by Olig3 bHLH transcription factor. *J. Neurosci.* **28**, 10124–10133.

Liu, Z.-R., Shi, M., Hu, Z.-L., Zheng, M.-H., Du, F., Zhao, G. and Ding, Y.-Q. (2010). A refined map of early gene expression in the dorsal rhombomere 1 of mouse embryos. *Brain Res. Bull.* **82**, 74–82.

Lu, X., Le Noble, F., Yuan, L., Jiang, Q., De Lafarge, B., Sugiyama, D., Bréant, C., Claes, F., De Smet, F., Thomas, J.-L., et al. (2004). The netrin receptor UNC5B mediates guidance events controlling morphogenesis of the vascular system. *Nature* **432**, 179–186.

Machold, R. and Fishell, G. (2005). Math1 is expressed in temporally discrete pools of cerebellar rhombic-lip neural progenitors. *Neuron* **48**, 17–24.

Marillat, V., Sabatier, C., Failli, V., Matsunaga, E., Sotelo, C., Tessier-Lavigne, M. and Chédotal, A. (2004). The slit receptor Rig-1/Robo3 controls midline crossing by hindbrain precerebellar neurons and axons. *Neuron* **43**, 69–79.

Matei, V., Pauley, S., Kaing, S., Rowitch, D., Beisel, K. W., Morris, K., Feng, F., Jones, K., Lee, J. and Fritzsch, B. (2005). Smaller inner ear sensory epithelia in Neurog 1 null mice are related to earlier hair cell cycle exit. *Dev. Dyn.* **234**, 633–650.

Miyahara, M., Shirasaki, R., Tashiro, Y., Muguruma, K., Heizmann, C. W. and Murakami, F. (2003). Pathfinding and growth termination of primary trigeminal sensory afferents in the embryonic rat hindbrain. *J. Comp. Neurol.* **460**, 503–513.

Mo, Z., Li, S., Yang, X. and Xiang, M. (2004). Role of the Barhl2 homeobox gene in the specification of glycinergic amacrine cells. *Development* **131**, 1607–1618.

Moreno-Bravo, J. A., Roig Puiggros, S., Blockus, H., Dominici, C., Zelina, P., Mehlen, P. and Chédotal, A. (2018). Commissural neurons transgress the CNS/PNS boundary in absence of ventricular zone-derived netrin 1. *Development* **145**, dev.159400.

Nichols, D. H. and Bruce, L. L. (2006). Migratory routes and fates of cells transcribing the Wnt-1 gene in the murine hindbrain. *Dev. Dyn.* **235**, 285–300.

Paxinos, G. (2004). *The Rat Nervous System*. 3rd ed. Gulf Professional Publishing.

Paxinos, G., Koutcherov, Y., Wang, H., Halliday, G. M. and Watson, C. (2006). *Atlas of the Developing Mouse Brain at E17.5, P0 and P6*. 1st ed. Oxford: Elsevier.

Paxinos, G., Xu-Feng, H., Sengul, G. and Watson, C. (2012). *Organization of Brainstem Nuclei*. *The Human Nervous System*. 3rd ed. Oxford: Elsevier.

Persson, M., Stamataki, D., Welscher, te, P., Andersson, E., Böse, J., Rüther, U., Ericson, J. and Briscoe, J. (2002). Dorsal-ventral patterning of the spinal cord requires Gli3 transcriptional repressor activity. *Genes Dev.* **16**, 2865–2878.

Philippidou, P. and Dasen, J. S. (2013). Hox genes: choreographers in neural development, architects of circuit organization. *Neuron* **80**, 12–34.

Przyborski, S. A., Knowles, B. B. and Ackerman, S. L. (1998). Embryonic phenotype of Unc5h3 mutant mice suggests chemorepulsion during the formation of the rostral cerebellar boundary. *Development* **125**, 41–50.

Ray, R. S. and Dymecki, S. M. (2009). Rautenlippe Redux -- toward a unified view of the precerebellar rhombic lip. *Curr. Opin. Cell Biol.* **21**, 741–747.

Renier, N., Wu, Z., Simon, D. J., Yang, J., Ariel, P. and Tessier-Lavigne, M. (2014). iDISCO: a simple, rapid method to immunolabel large tissue samples for volume imaging. *Cell* **159**, 896–910.

Rétaux, S., Rogard, M., Bach, I., Failli, V. and Besson, M. J. (1999). Lhx9: a novel LIM-homeodomain gene expressed in the developing forebrain. *J. Neurosci.* **19**, 783–793.

Rodriguez, C. I. and Dymecki, S. M. (2000). Origin of the precerebellar system. *Neuron* **27**, 475–486.

Roy, A., Francius, C., Rousso, D. L., Seuntjens, E., Debruyn, J., Luxenhofer, G., Huber, A. B., Huylebroeck, D., Novitch, B. G. and Clotman, F. (2012). Onecut transcription factors act upstream of Isl1 to regulate spinal motoneuron diversification. *Development* **139**, 3109–3119.

Saba, R., Nakatsuji, N. and Saito, T. (2003). Mammalian BarH1 confers commissural neuron identity on dorsal cells in the spinal cord. *J. Neurosci* **23**, 1987–1991.

Schambra, U. (2008). *Prenatal Mouse Brain Atlas*. Boston, MA: Springer US.

Shinohara, M., Zhu, Y. and Murakami, F. (2013). Four-dimensional analysis of nucleogenesis of the pontine nucleus in the hindbrain. *J. Comp. Neurol.* **521**, 3340–3357.

Soriano, P. (1999). Generalized lacZ expression with the ROSA26 Cre reporter strain. *Nat Genet* **21**, 70–71.

Srinivas, S., Watanabe, T., Lin, C.-S., William, C. M., Tanabe, Y., Jessell, T. M. and Costantini, F. (2001). Cre reporter strains produced by targeted insertion of EYFP and ECFP into the ROSA26 locus. *BMC Dev. Biol.* **1**, 4.

Steventon, B., Mayor, R. and Streit, A. (2014). Neural crest and placode interaction during the development of the cranial sensory system. *Dev. Bio.* **389**, 28–38.

Storm, R., Cholewa-Waclaw, J., Reuter, K., Bröhl, D., Sieber, M., Treier, M., Müller, T. and Birchmeier, C. (2008). The bHLH transcription factor Olig3 marks the dorsal neuroepithelium of the hindbrain and is essential for the development of brainstem nuclei. *Development* **136**, 295-305.

Sudarov, A., Kim, E. J., Lebel-Potter, M., Guillemot, F. and Joyner, A. L. (2011). Ascl1 Genetics Reveals Insights into Cerebellum Local Circuit Assembly. *Neural Dev.* **31**, 11055–11069.

Ter-Avetisyan, G., Dumoulin, A., Herrel, A., Schmidt, H., Strump, J., Afzal, S. and Rathjen, F. G. (2018). Loss of Axon Bifurcation in Mesencephalic Trigeminal Neurons Impairs the Maximal Biting Force in Npr2-Deficient Mice. *Front. Cell. Neurosci.* **12**, 1271–15.

Theil, T., Alvarez-Bolado, G., Walter, A. and Rüther, U. (1999). Gli3 is required for Emx gene expression during dorsal telencephalon development. *Development* **126**, 3561–3571.

Tissir, F., Wang, C.-E. and Goffinet, A. M. (2004). Expression of the chemokine receptor Cxcr4 mRNA during mouse brain development. *Brain Res. Dev. Brain Res.* **149**, 63–71.

Tronche, F., Kellendonk, C., Kretz, O., Gass, P., Anlag, K., Orban, P. C., Bock, R., Klein, R. and Schütz, G. (1999). Disruption of the glucocorticoid receptor gene in the nervous system results in reduced anxiety. *Nat. Genet*. **23**, 99–103.

Ulloa, F. and Martí, E. (2010). Wnt won the war: antagonistic role of Wnt over Shh controls dorso-ventral patterning of the vertebrate neural tube. *Dev. Dyn.* **239**, 69–76.

Ulloa, F., Itasaki, N. and Briscoe, J. (2007). Inhibitory Gli3 activity negatively regulates Wnt/beta-catenin signaling. *Curr. Biol.* **17**, 545–550.

Wang, V. Y., Rose, M. F. and Zoghbi, H. Y. (2005). Math1 expression redefines the rhombic lip derivatives and reveals novel lineages within the brainstem and cerebellum. *Neuron* **48**, 31–43.

Watson, C. Paxinos, G. and Puelles L. (2012). The mouse nervous system. The hindbrain. 1st ed. Academic Press Elsevier

Willaredt, M. A., Hasenpusch-Theil, K., Gardner, H. A. R., Kitanovic, I., Hirschfeld-Warneken, V. C., Gojak, C. P., Gorgas, K., Bradford, C. L., Spatz, J., Wölfl, S., et al. (2008). A crucial role for primary cilia in cortical morphogenesis. *J. Neurosci.* **28**, 12887–12900.

Wingate, R. J. (2001). The rhombic lip and early cerebellar development. *Curr. Opin. Neurobiol.* **11**, 82–88.

Xiang, M., Gan, L., Zhou, L., Klein, W. H. and Nathans, J. (1996). Targeted deletion of the mouse POU domain gene Brn-3a causes selective loss of neurons in the brainstem and trigeminal ganglion, uncoordinated limb movement, and impaired suckling. *Proc Natl Acad Sci USA* **93**, 11950–11955.

Yamada, M., Terao, M., Terashima, T., Fujiyama, T., Kawaguchi, Y., Nabeshima, Y.-I. and Hoshino, M. (2007). Origin of Climbing Fiber Neurons and Their Developmental Dependence on Ptf1a. *J. Neurosci.* **27**, 10924–10934.

Yamauchi, K., Yamazaki, M., Abe, M., Sakimura, K., Lickert, H., Kawasaki, T., Murakami, F. and Hirata, T. (2017). Netrin-1 Derived from the Ventricular Zone, but not the Floor Plate, Directs Hindbrain Commissural Axons to the Ventral Midline. *Sci. Rep.* **7**, 11992.

Yung, A. R., Druckenbrod, N. R., Cloutier, J.-F., Wu, Z., Tessier-Lavigne, M. and Goodrich, L. V. (2018). Netrin-1 Confines Rhombic Lip-Derived Neurons to the CNS. *CellReports* **22**, 1666–1680.

Zelina, P., Blockus, H., Zagar, Y., Péres, A., Friocourt, F., Wu, Z., Rama, N., Fouquet, C., Hohenester, E., Tessier-Lavigne, M., et al. (2014). Signaling Switch of the Axon Guidance Receptor Robo3 during Vertebrate Evolution. *Neuron* **84**, 1258–1272.

Zhu, Y. and Guthrie, S. (2002). Expression of the ETS transcription factorER81 in the developing chick and mouse hindbrain. *Dev. Dyn.* **225**, 365–368.

Zhu, Y., Matsumoto, T., Mikami, S., Nagasawa, T. and Murakami, F. (2009). SDF1/CXCR4 signalling regulates two distinct processes of precerebellar neuronal migration and its depletion leads to abnormal pontine nuclei formation. *Development* **136**, 1919–1928.

Figures

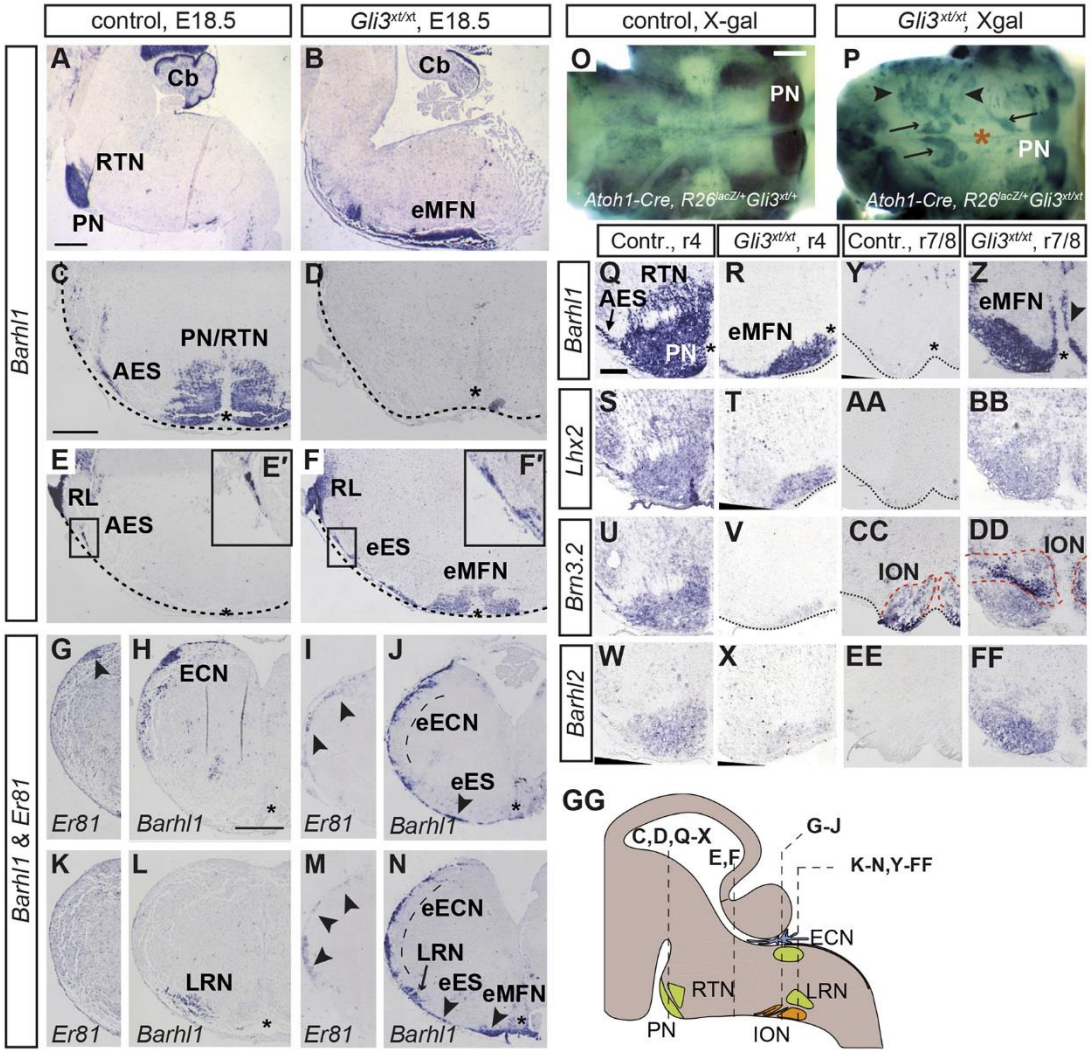

Figure 1: MF nuclei are disorganized in *Gli3*$^{xt/xt}$ mutants. (A-F) *In situ* hybridization for the MFN marker *Barhl1*. In *Gli3*$^{xt/xt}$ mutants, the PN/RTN are not formed at their correct position in r4 (A-D). Ectopic MFN clusters (eMFN) and an ectopic extramural stream (eES) form in *Gli3*$^{xt/xt}$ mutants. Remnants of the AES are present in controls (E,F). Sagittal (A,B) and coronal sections (C-F). (G-N) *In situ* hybridization for *Barhl1* and *Er81*. *Barhl1*- and *Er81*-double-positive cells form the ECN in controls, but are spread out extramurally in *Gli3*$^{xt/xt}$ mutants (eECN, arrowheads/dashed line) (G-J,M,N). A rudimentary *Barhl1*-positive LRN is visible in the mutants (K-N). An eES in the ventral hindbrain and clusters of eMFN at the ventral midline are present in the mutants. The rostrocaudal level of the sections is indicated in (GG). Number of embryos analyzed: 9 controls, 5 mutants (A,B); 20 controls, 15 mutants for *Barhl1*; 5 controls, 3 mutants for *Er81* (C-N). (O,P) Whole mount X-gal staining of E18.5 *Atoh1-Cre; R26*$^{lacz/+}$ brains, ventral view. Neurons derived from *Atoh1*-expressing RL cells

are disorganized in *Gli3*$^{xt/xt}$ mutants. The PN is partially formed in this mutant. Arrowheads: ectopic cell streams. Arrows: ectopic cell clusters. 1 control and 1 mutant embryo were analyzed. (Q-FF) *In situ* hybridization for *Barhl1, Lhx2*, *Brn3.2* and *Barhl2* on adjacent sections at E18.5. In *Gli3*$^{xt/xt}$ mutant brains, eMFN in r7/8 express PN/RTN marker *Barhl1* and *Lhx2* and PN marker *Brn3.2* and *Barhl2* (Y-FF). The thin layer of *Barhl1*-positive cells (arrowhead) on both sides of the midline are negative for these markers. The clustered cells in r4 show weak expression of *Brn3.2* and *Barhl2* (Q-X). Asterisks indicate the ventral midline. The rostrocaudal level of the sections is indicated in (GG). Number of embryos analyzed: 3 controls, 4 mutants. (GG) Schematic of the hindbrain. Scale bars: 200 μm (A-N; Q-FF), 400 μm (O,P).

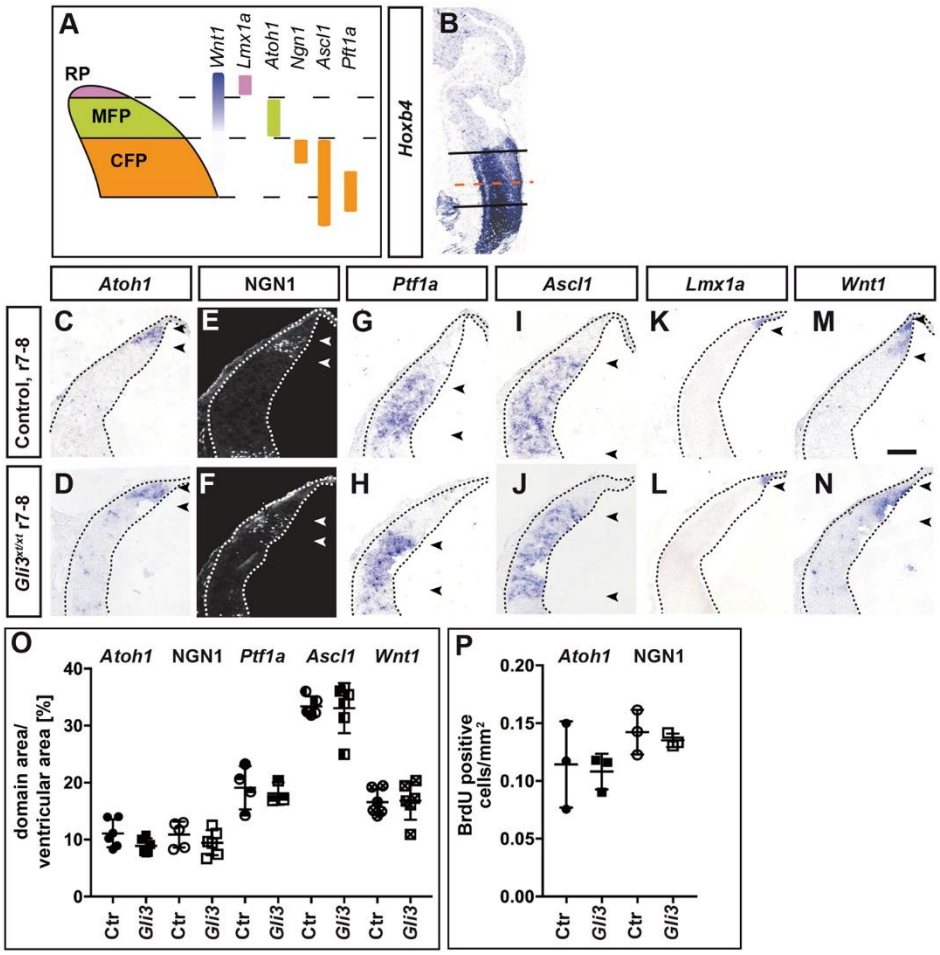

Figure 2: MF and CF progenitor domains are not altered in *Gli3*$^{xt/xt}$ mutants. (A) Schematic summarizing gene expression in MF and CF progenitor (MFP and CFP) domains. (B) *Hoxb4* staining marks r7/r8 and spinal cord; sagittal section. Red dashed line: level used for quantification in (O and P). (C-J) *In situ* hybridization (C,D,G-J) and immunostaining (E,F) for MFPs (*Atoh1* positive) and CFPs (*Ptf1a*, *Ascl1*, NGN1 positive) show that that the RL progenitor domains are unaffected in the mutants. (K,L) *Lmx1a* expression shows that the roof plate is established in E10.5 *Gli3*$^{xt/xt}$ embryos. (M,N) *Wnt1* domains in the *Gli3*$^{xt/xt}$ hindbrain are comparable to the domains in the controls. (O) Quantification of progenitor domain size (normalized to the size of the ventricle). Number of embryos analyzed: *Wnt1*: 6 controls, 6 mutants; *Atoh1*: 6 controls, 6 mutants; *Ptf1a*: 4 controls, 3 mutants; NGN1: 5 controls, 6 mutants, *Ascl1*: 6 controls, 6 mutants. Significance was assessed with Kurskal-Wallis test. *Lmx1a* expression was analyzed on 2 control and 2 mutant embryos. (O) Quantification of BrdU-positive cells (1-hour BrdU pulse) within the *Atoh1* and NGN1 domain shows no significant difference between control and *Gli3*$^{xt/xt}$ mutant embryos (n=3 embryos for both control and mutant, two tailed Student's t-test). (O,P) Values are represented as mean ± SD. Scale bar: 50 µm.

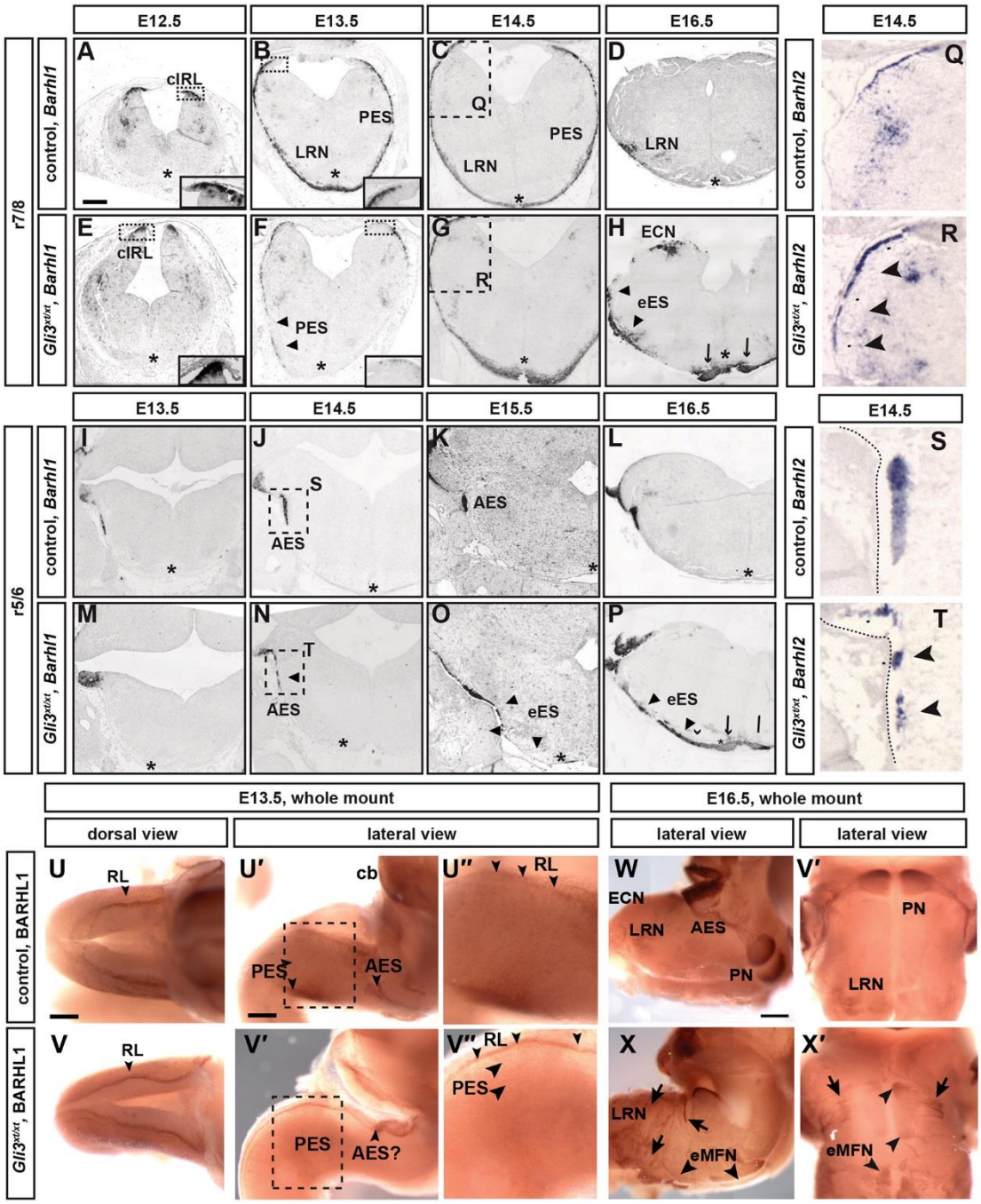

Figure 3: AES and PES are delayed and localized at ectopic positions in *Gli3*$^{xt/xt}$ hindbrain. (A-P) *In situ* hybridization for *Barhl1* between E12.5 and E16.5. (A-H) PES and AES in r7/r8. The *Gli3*$^{xt/xt}$ PES reaches the midline with a delay of one day relative to controls (A-C,E-G). (A,B,E,F) Dotted boxes indicate the area shown in the lower right corner. (C,G) Dashed boxes indicate the area shown in (Q) and (R). (D,H) At E16.5, the LRN has formed in controls. The ECN is not visible at this level. In *Gli3*$^{xt/xt}$ mutants, PES cells remain partially in an extramural position (ectopic extramural stream, eES, arrowheads), and the ECN starts to form. Ectopic clusters of MFN form at the ventral midline (arrows). (I-P) At E13.5, a compact

AES has formed in r5 of control but not of *Gli3*$^{xt/xt}$ mutant embryos (I,M). By E14.5, the AES is present in the mutants, but is more dispersed than in controls (J,N, boxed area). Boxes indicate the area shown in (S) and (T). In the mutants, the AES extends further ventrally at E15.5 (eES, arrowheads) and reaches the ventral midline by E16.5. Ectopic MFN clusters (arrows) have formed (O,P). *Barhl1*-positive clusters remain in an extramural position (eES, arrowheads) (P). Asterisks indicate ventral midline. (Q-T) *Barhl2* marks the AES in controls. In *Gli3*$^{xt/xt}$ mutants, *Barhl2*-expression extends towards the ventral hindbrain at the r7/8 level (R) and is fragmented at the r5 level (T). Number of embryos analyzed for *Barhl1*: 4 controls, 4 mutants at E12.5; 3 controls, 4 mutants at E13.5; 16 controls, 10 mutants at E14.5; 2 controls, 2 mutants at E16.5. For *Barhl2*: 8 controls, 6 mutants at E14.5; (U-X) Whole-mount immunostaininig for BARHL1 at E13.5 (U-V″) and E16.5 (W-X′) shows the delayed onset and disorganization of the MFN migratory streams (arrows) and the ectopic accumulation of MFN cells (eMFN, arrowheads) along the rostrocaudal axis in the *Gli3*$^{xt/xt}$ mutant hindbrain. U″,V″ are higher magnifications of the boxed area in U′,V′. In the E13.5 *Gli3*$^{xt/xt}$ mutant hindbrain the PES is only weakly stained for BARHL1, consistent with the analysis in sections, in which the PES is thinner or barely present in E13.5 mutants (in F). Note that some of the whole-mount pictures are composed of two stitched images to have the entire hindbrain in focus. Number of embryos analyzed: E13.5: n=8 controls, n=2 mutants, E16.5: n=4 controls, n=3 mutants. cb: cerebellum. Scale bar: 200 μm (A- X′).

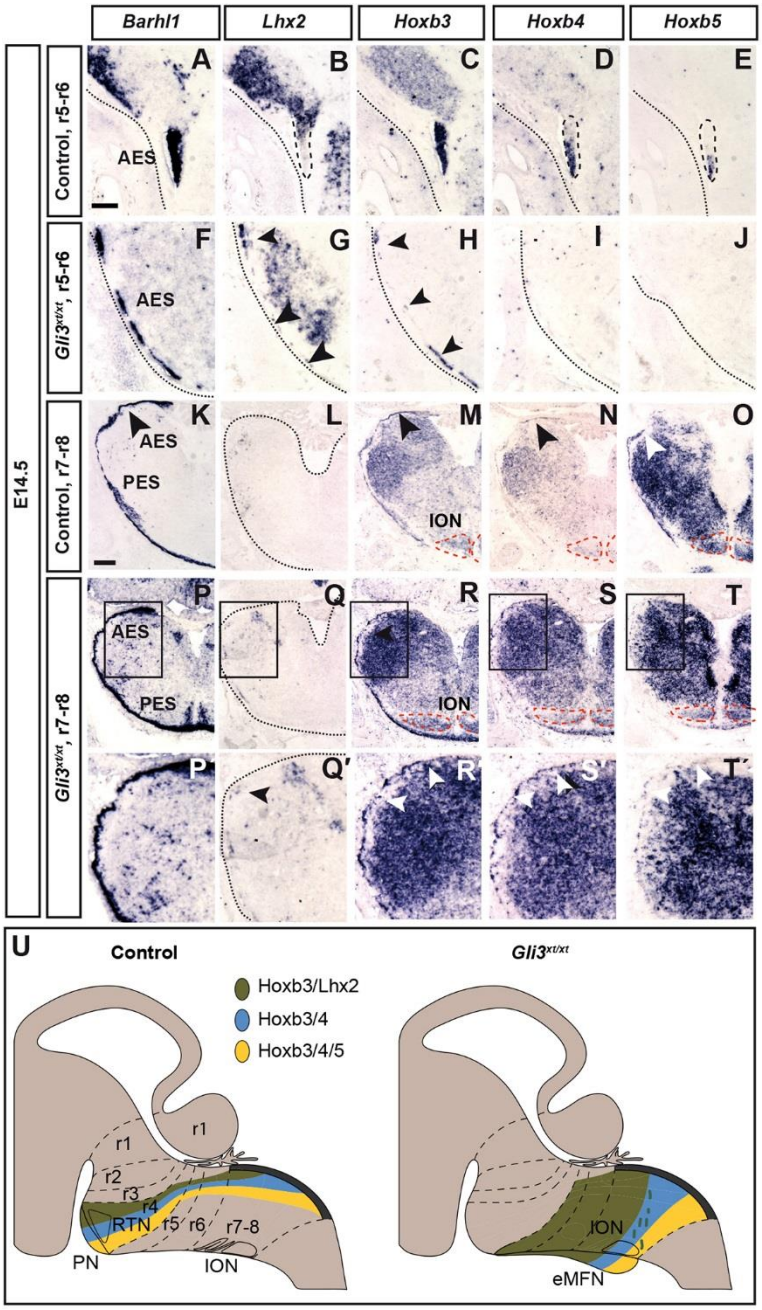

Figure 4: The r7/8-derived portion of the AES fails to turn rostrally in *Gli3*$^{xt/xt}$ mutants. *In situ* hybridization for *Barhl1, Lhx2, Hoxb3, Hoxb4* and *Hoxb5* at E14.5. (A-E) In control hindbrain, the AES (dashed outline) is organized from dorsal-to-ventral according to the rhombomeric-origin of the cells and is defined by specific combinations of Hox-gene expression: the dorsal AES is *Hoxb3* positive (r6-derived), the intermediate AES is *Hoxb3/4* positive (r7-derived), the ventral AES is *Hoxb3/4/5* positive (r8-derived). The dorsal (*Hoxb3*-only) AES is also *Lhx2* positive. (F-J) In *Gli3*$^{xt/xt}$ mutants, the AES in r5/6 contains cells that are *Hoxb3*/*Lhx2* positive (F-H, arrowheads), but *Hoxb4/5* negative (I,J). (K-T′) In r8, the emerging AES cells express *Hoxb3/4/5* in controls and in *Gli3*$^{xt/xt}$ mutants. Dashed red line: outline of ION. (K-O)

Arrowheads indicate AES (K-O), *Lhx2* positive AES cells (Q, Q') or *Hoxb3/4/5*-expression in the AES. (U) Schematic summarizing the *Hoxb* expression patterns in the AES. Number of embryos analyzed: 5 controls, 4 mutants for *Lhx2*; 8 controls, 7 mutants for *Hoxb3/4/5*. Scale bars: 100 μm (A-J); 200 μm (K-T).

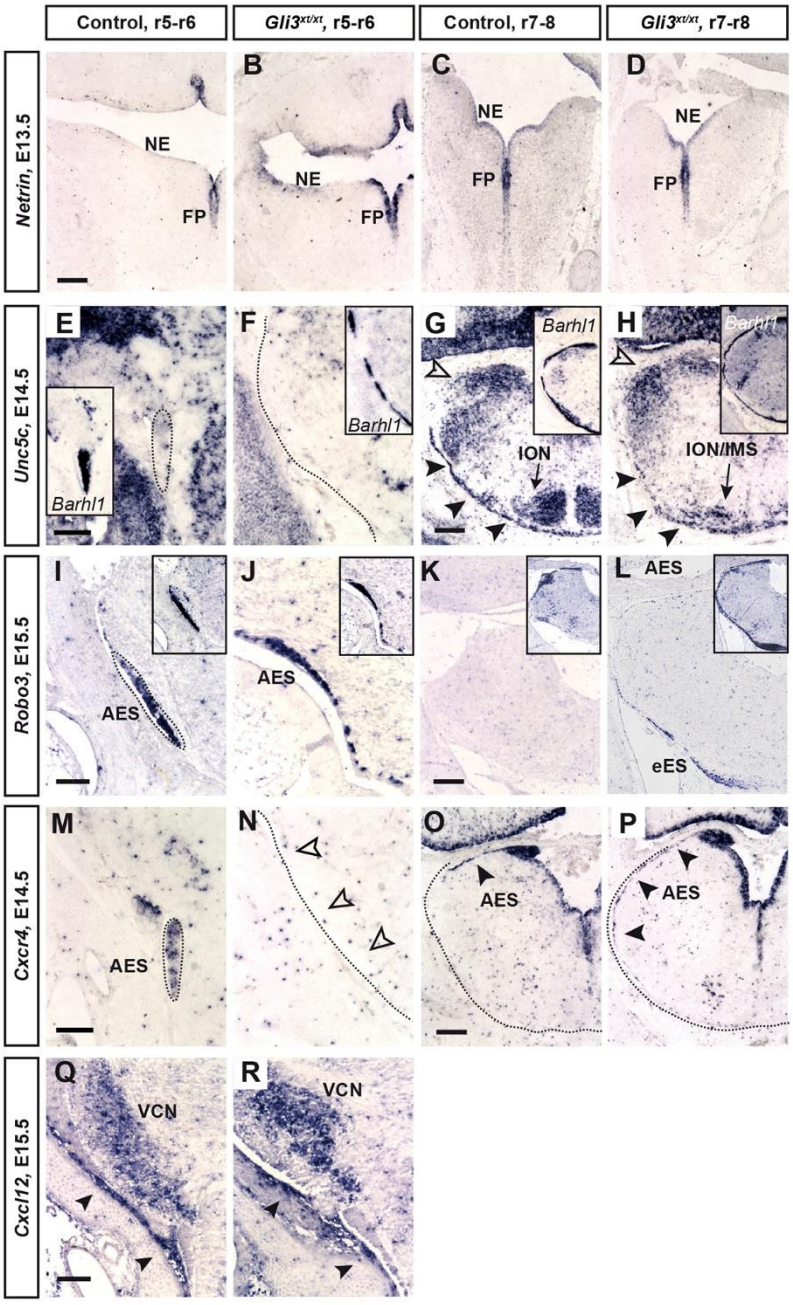

Figure 5: Expression of guidance molecules and receptors in the *Gli3*$^{xt/xt}$ hindbrain. *In situ* hybridization for *Netrin1* and the receptors *Unc5c* and *Robo3,* as well as for *Cxcl12* and its receptor *Cxcr4* at E13.5 - E15.5. (A-D) Expression of *Netrin* in the hindbrain floor plate (FP) and neuroepithelium (NE) is comparable in E13.5 controls (n=3 embryos) and *Gli3*$^{xt/xt}$ embryos (n=3 embryos). (E-H) In E14.5 control and *Gli3*$^{xt/xt}$ mutant brains, *Unc5c* is expressed in the PES (filled arrowheads) and ION/IMS (arrows), but not in the AES (unfilled arrowheads). Inserts in E-H depict *Barhl1* expression on sections adjacent to E-H and M-P. 3 control and 3 mutant embryos were analyzed. (I-L) *Robo3* is strongly expressed throughout the AES in controls and in the AES and eES in r5/6 and r7/8 of *Gli3*$^{xt/xt}$ mutants at E15.5. 3 control and 3 mutant embryos were analyzed. (M-P) *Cxcr4* is expressed in the AES

in E14.5 control brains (AES outlined in M, filled arrowhead in O, n=4 embryos). In *Gli3*$^{xt/xt}$ brains (n=4 embryos), *Cxcr4* expression is excluded from the rostral AES (N, unfilled arrowheads), while it is expressed in the eES at r7/8 levels (P, filled arrowheads). (Q,R) The chemokine *Cxcl12* is expressed in meninges (arrowheads) and in the ventral cochlear nucleus (VCN) in E15.5 control (n=3 embryos) and mutant hindbrain (n=3 embryos). Scale bars: 200 μm (A-D,G,H,K,L,O,P); 100 μm (E,F,I,J,M,N,Q,R).

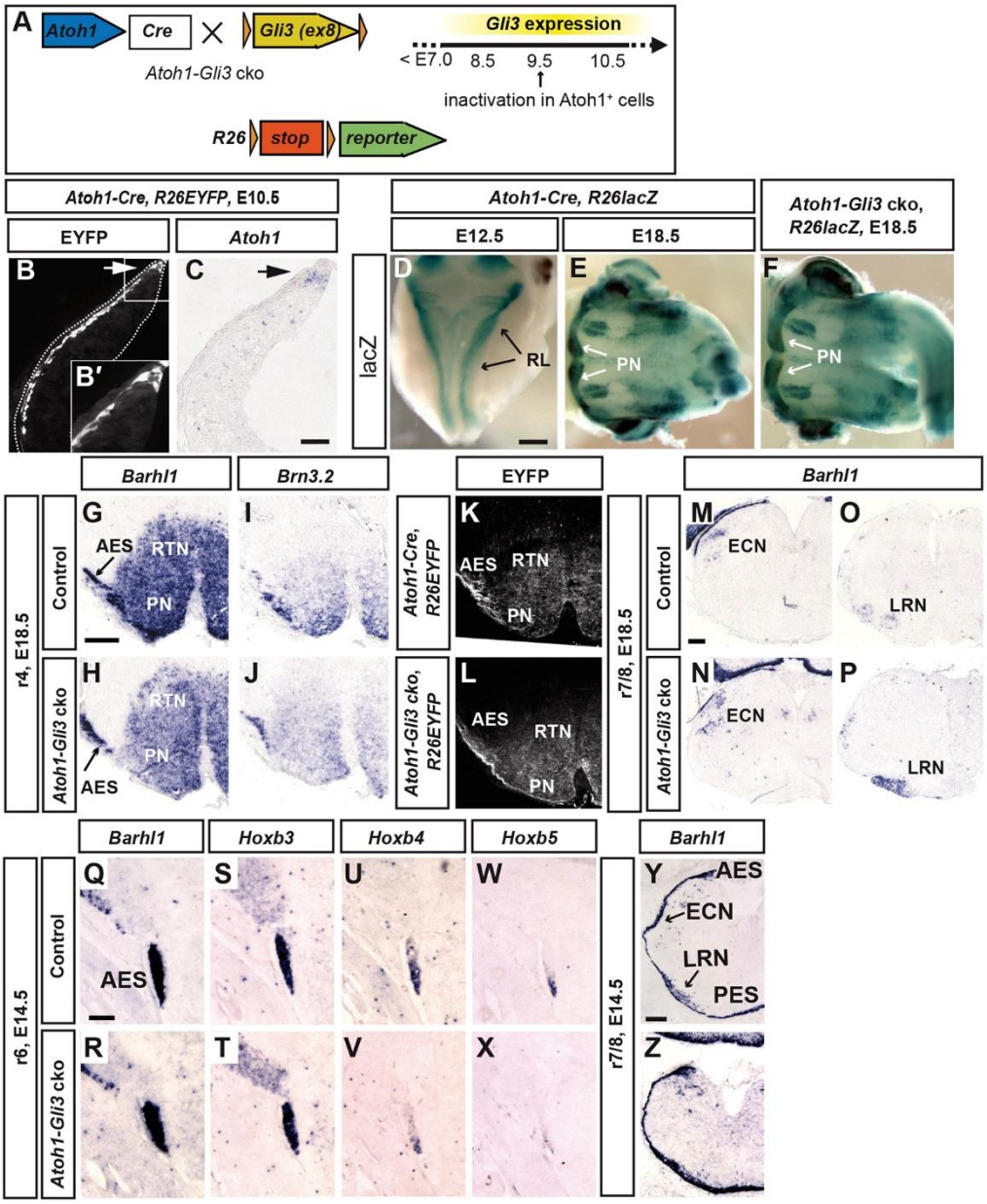

Figure 6: Inactivation of *Gli3* in MF progenitors does not result in defects in AES, PES and MF nuclei. (A) Conditional inactivation of *Gli3* in *Atoh1*-expressing progenitors (*Atoh1-Gli3* cko) combined with a R26 reporter allele. (B,C) *Atoh1-Cre* mice were crossed with a *R26-EYFP* reporter mouse. Immunostaining for EYFP (B) and *in situ* hybridization for *Atoh1* in coronal sections of the E10.5 caudal hindbrain. Inset in B: higher magnification of the boxed area. 3 embryos were analyzed. (D,E) *Atoh1-Cre* mice crossed with a *R26-lacZ* reporter mouse. Whole mount staining for X-gal shows recombination in the RL at E12.5 and in RL-derived nuclei at E18.5. (F) E18.5 X-gal staining of whole mount brains of *Atoh1-Gli3* cko mice on a *R26lacZ* background. RL-derived nuclei are formed in *Gli3*$^{xt/xt}$ mutants. 3 control embryos were analyzed at E12.5 and E18.5, 1 mutant at E18.5. (G-P) MF nuclei are

correctly established in the hindbrain of E18.5 *Atoh1-Gli3* cko mice. *In situ* hybridization for *Barhl1* and *Brn3.2* to label PN/RTN in r4 (G-J, coronal sections) and for *Barhl1* to label ECN and LRN in r7/8 (M-P, coronal sections). (K,L) Immunostaining for EYFP in coronal hindbrain sections of *Atoh1-Gli3* cko mice on a *R26EYFP* background. PN/RTN are EYFP-positive. 4 control and 4 mutant embryos were analyzed. (Q-Z) *In situ* hybridization for *Barhl1* and *Hoxb3/4/5* on E14.5 coronal sections shows that location and organization of AES and PES in *Atoh1-Gli3* cko mice are comparable to controls. 8 control and 4 mutant embryos were analyzed. Scale bars: 50 μm (B,C); 500 μm (D-F); 200 μm (G-P,Y,Z); 100 μm (Q-X).

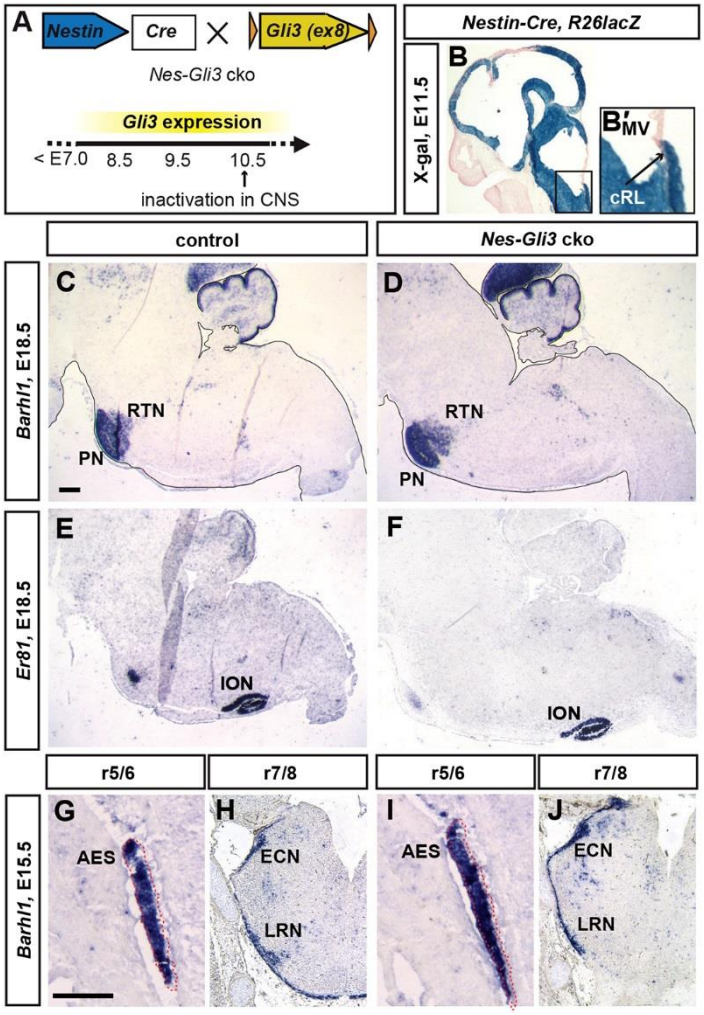

Figure 7. Inactivation of *Gli3* in neural progenitors after E10.5 does not result in defects in the precerebellar system. (A) Conditional knock-out of *Gli3* in the CNS using *Nestin*-Cre mice (*Nes-Gli3* cko). (B) *Nestin-Cre* mice were crossed with a *R26-lacZ* reporter mouse. X-gal staining on E11.5 sagittal sections shows recombination in the caudal rhombic lip (cRL) but not in the medullary velum (MV). Inset in B: higher magnification of the boxed area. n=2 embryos. (C-F) *In situ* hybridization for *Barhl1* and *Er81* at E18.5. ION and MF nuclei are established at their correct positions in the hindbrain of E18.5 *Nes-Gli3* cko mice. (G-J) *In situ* hybridization for *Barhl1* on E15.5 coronal sections. AES and PES develop normally in *Nes-Gli3* cko mice. 3 control and 3 mutant embryos were analyzed at E15.5 and at E18.5. Scale bars: 200 μm (B -F); 100 μm (G-J).

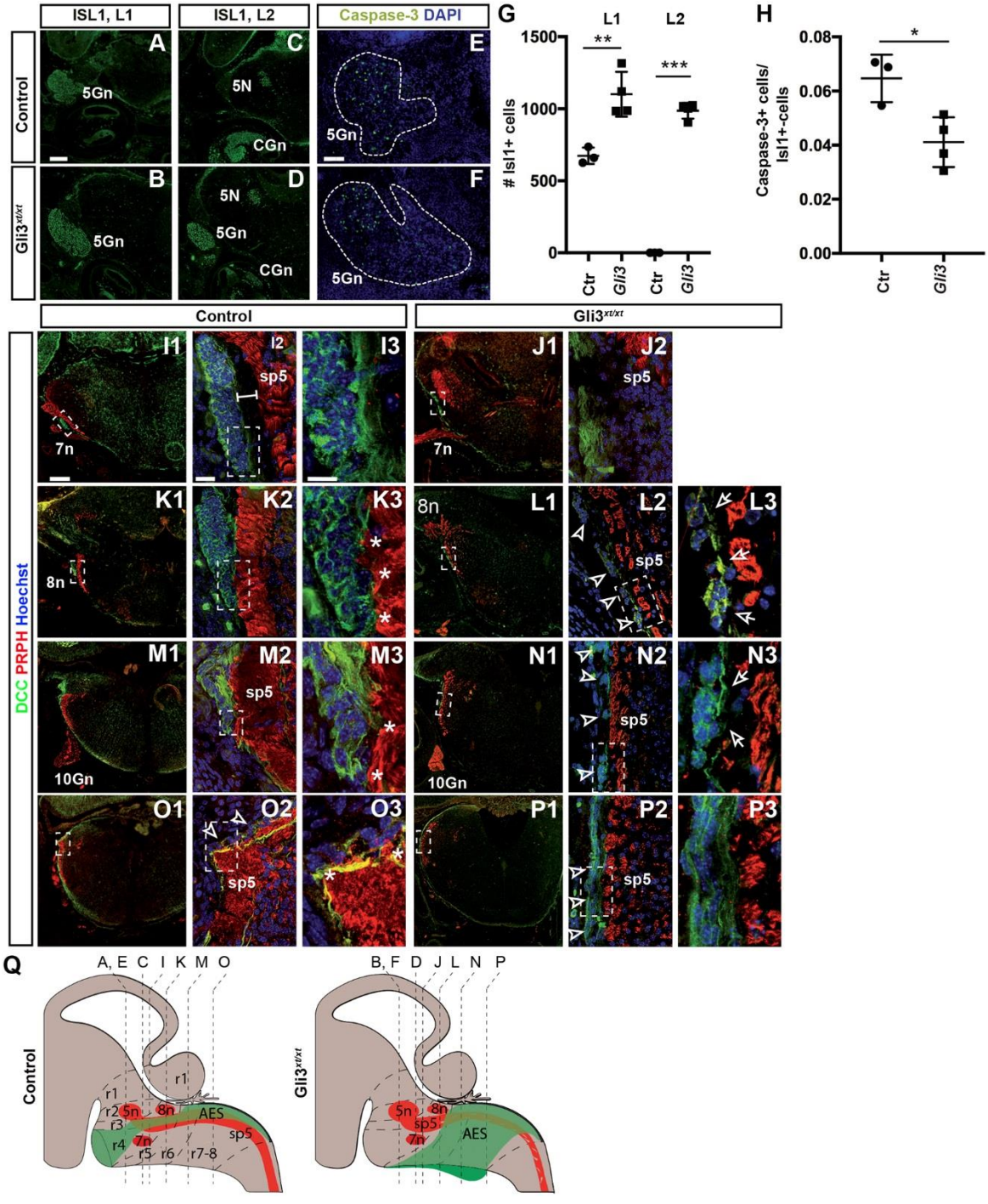

Figure 8. Rostrally-migrating AES neurons are in close contact with the spinal trigeminal tract, which is disorganized in *Gli3*$^{xt/xt}$ mutants. (A-F) *Gli3* inactivation results in a caudal expansion of the trigeminal ganglia (5Gn) and reduced cell death in 5Gn. E14.5 coronal slides, immunostaining for ISL1 (A-D) and cleaved caspase-3 (E,F). (G,H) Quantification of ISL1+ cells (G) and of cleaved caspase-3 positive cells in 5Gn; 3 controls and 4 mutant embros. *p<0.05, **p<0.01, ***p<0.01, two-tailed Student's t-test. Values are represented as mean ± SD. (I1-P3) AES and the spinal trigeminal tract (sp5). E14.5 coronal slides, immunostaining for PRPH and DCC. In the control, the DCC-positive AES is positioned close to the sp5 before (O, asterisks in O3) and during the rostral phase of migration (K,M) and separates from the sp5 during the final ventral phase of migration in r3/r4 (I). Cells in the ventral AES appear to be in direct contact with the sp5 during their rostral migration (K3,M3, asterisks). In *Gli3*$^{xt/xt}$ mutants, the sp5 is disorganized and increased in size at rostral levels (J) but thinned out and less fasciculated at caudal levels (L,N,P). The AES is fragmented in small clusters (arrowheads in L2,N2,P2) and detached from the sp5 (arrows in L3,N3,P3). At the r3/r4 level, the AES is not visible in the mutants (J2), thus no higher magnification is shown. (I3-P3) Maximum intensity projections of Z-stacks acquired with structured illumination. 3 control and 3 mutant embryos were analyzed. (Q) Summary schematic. 5n, trigeminal nerve; 5N, motor trigeminal nucleus; 7n, facial nerve; 8n; vestibulocochlear nerve; 10Gn, vagus nerve ganglion; CGn, cochlear (spiral) ganglion. Scale bars: 200 µm (A-D; I1-P1), 100 µm (E,F), 25 µm (I2-P2), 12.5 (I3-P3) µm.

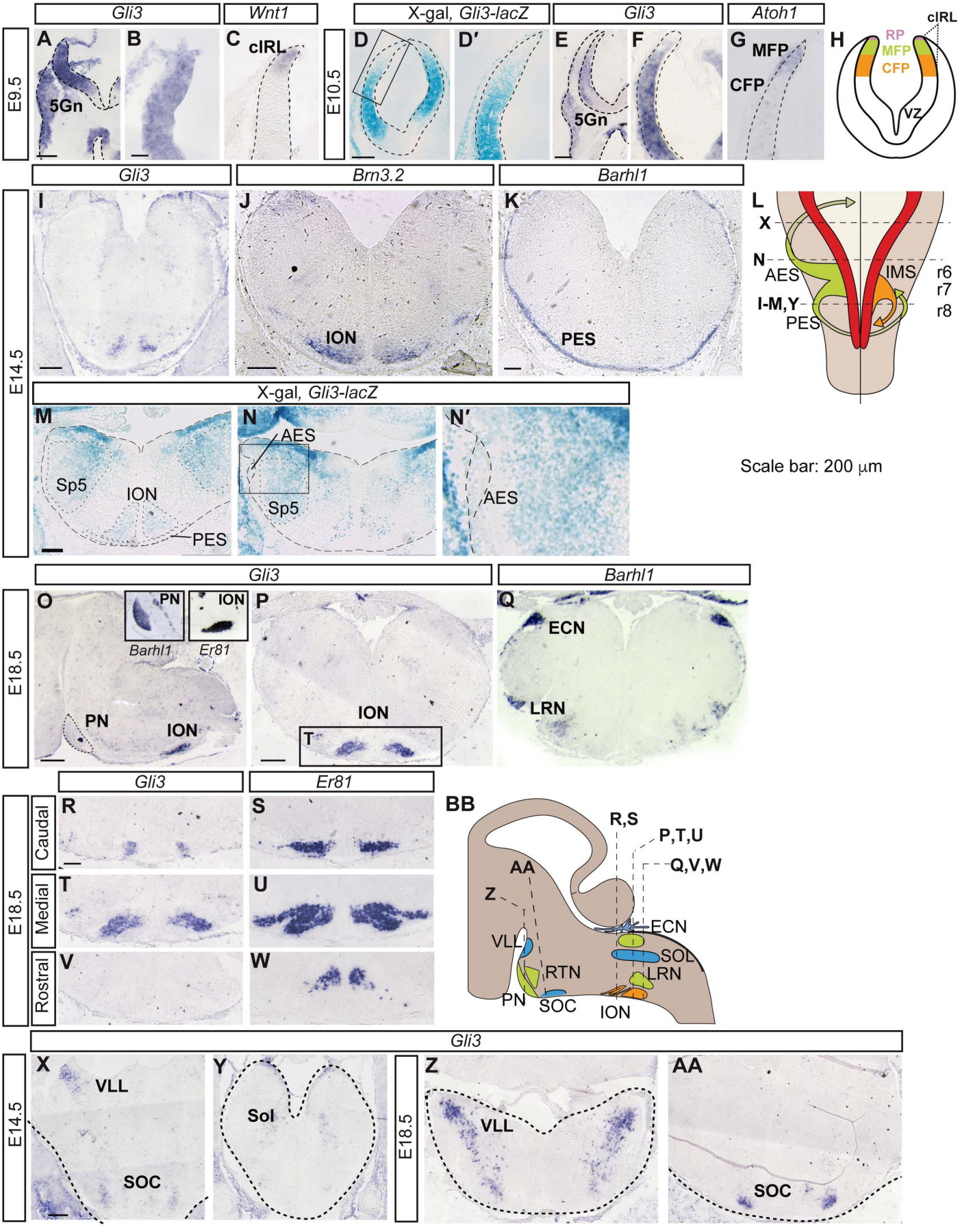

Figure S1: *Gli3* expression in the embryonic hindbrain. (A-C) *In situ* hybridization for *Gli3* and *Wnt1* at E9.5. *Gli3* is expressed throughout the dorsal hindbrain including the *Wnt1*-expressing caudal lower rhombic lib (clRL). *Gli3* is also expressed in the forming trigeminal ganglia (5Gn). n=2 embryos. (D-G) X-gal staining in sections from $Gli3^{lacZ/+}$ embryos and *in situ* hybridization for *Gli3* and *Atoh1.* At E10.5, *Gli3* is no longer expressed in the roof plate (RP) or MF progenitor domain (MFP) but is maintained in the CF progenitor domain (CFP). (D′) Higher magnification of the boxed area in D. (H) Schematic of the caudal hindbrain at E10.5. VZ: ventricular zone. n=3 embryos for in situ analysis, n=2 embryos for X-gal analysis. (I-K) *In situ* hybridization for *Gli3, Brn3.2* and *Barhl1* at E14.5; n=3 embryos. *Gli3* is expressed in a subdomain of the forming ION, but it is not expressed in the PES at E14.5. Rostrocaudal level of sections are indicated in (L). (L) Schematic depicting the precerebellar migratory streams. (M,N) X-gal staining in sections from E14.5 $Gli3^{lacZ/+}$ embryos showing expression of the reporter in the spinal trigeminal nucleus (Sp5) and ION. The AES is lacZ negative. (N′) Higher magnification of the boxed area in N. Rostrocaudal level of sections are indicated in (L). n=1 embryo. (O-W) *In situ* hybridization for *Gli3, Er81* and *Barhl1* at E18.5. At E18.5, *Gli3* is expressed in the *Er81*-positive ION subdomain (principal olivary nucleus). The MF nuclei (ECN, LRN, PN) are *Gli3*-negative. (T) Higher magnification of the boxed area in P. Rostrocaudal level of sections are indicated in (BB). (X-AA) *In situ* hybridization on coronal sections for *Gli3* at E14.5 (X,Y) and E18.5 (Z,AA). n=3 embryos. (BB) Schematic depicting the precerebellar nuclei and Gli3 expressing nuclei (blue). VLL: ventral nucleus of the lateral lemniscus, Sol: solitary nucleus, SOC: superior olivary complex. Scale bars: 50 μm (A,B); 100 μm (C-E, L-Q); 200 μm (F-K, U-X).

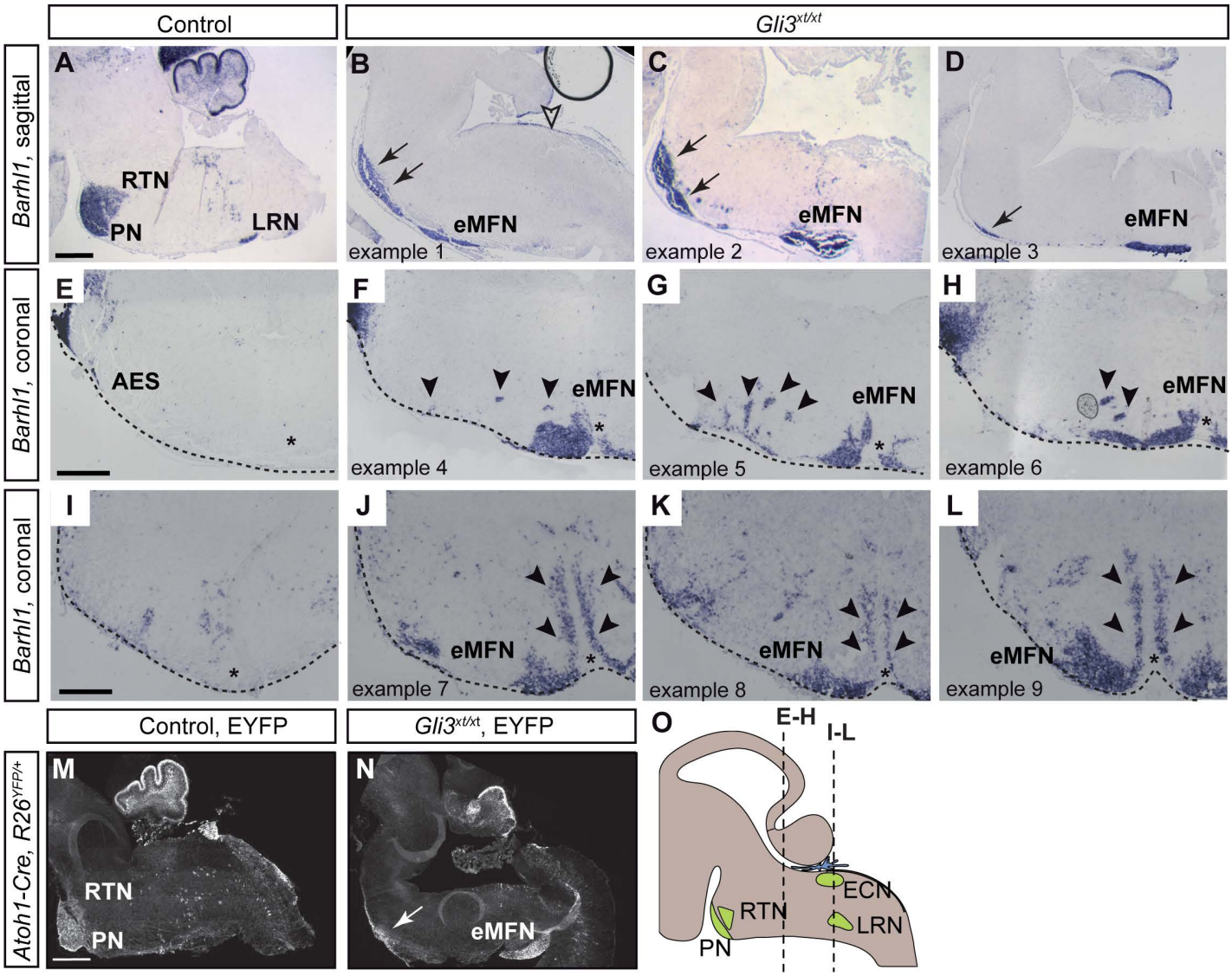

Figure S2: Variable phenotype of MF nuclei in *Gli3*$^{xt/xt}$ mutants. (A-H) *In situ* hybridization for the MFN marker *Barhl1* on sagittal (A-D) and coronal sections (E-L). In some *Gli3*$^{xt/xt}$ mutants, the PN and RTN are partially formed at their normal position in r4 (B-D, arrows). *Barhl1*-positive MFN clusters are in ectopic positions (eMFN) along the ventral midline (asterisks) of the hindbrain. (E-H) eMFN at the ventral midline (asterisks) at the r5/6 level in *Gli3*$^{xt/xt}$ mutants (F-H). Note the presence of small, more laterally located Barhl1-positive cell clusters (arrowheads), suggesting that cells delaminate ectopically from the AES in the *Gli3*$^{xt/xt}$ mutants. Observed in n=9/15 mutants. (I-L) eMFN at the ventral midline (asterisks) at the r7/8 level in *Gli3*$^{xt/xt}$ mutants. Note the stream of cells on both sides of the midline (arrowheads). (M,N) Immunostaining for GFP in sagittal sections of E18.5 *Atoh1-Cre; R26*$^{EYFP/+}$ brains. Neurons derived from *Atoh1*-expressing rhombic lip cells form eMFN in *Gli3*$^{xt/xt}$ mutants. Arrow indicates remnants of the PN/RTN. In some mutants (n=5/15), there is a strong asymmetry between the nuclei on both sides of the midline. (O) Schematic of the embryonic hindbrain. Level of sections in E-L are indicated. Scale bars: 400 µm.

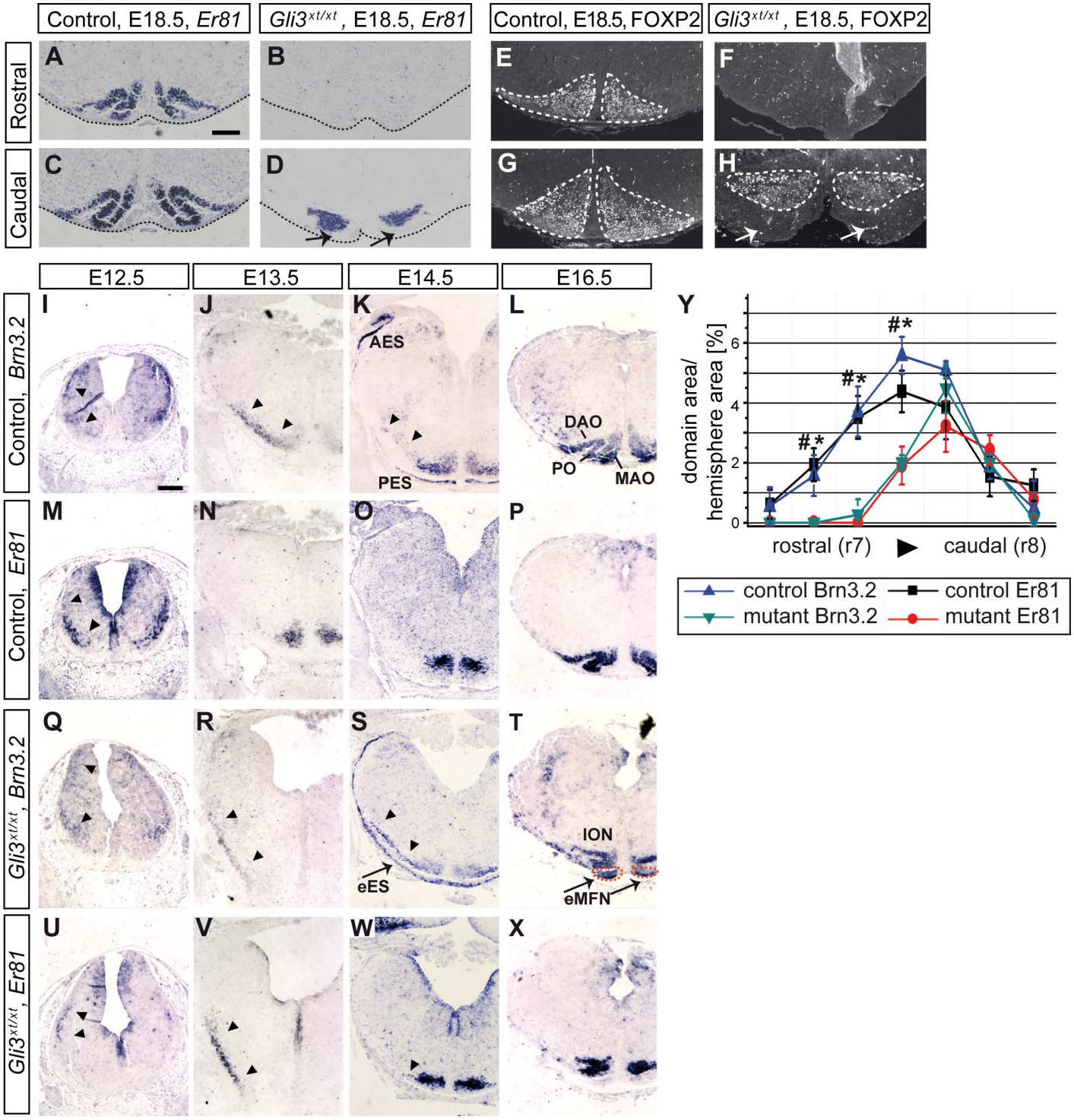

Figure S3: CFN migration and ION formation in *Gli3*$^{xt/xt}$ mutants. (A-H) *In situ* hybridization for *Er81* (A-D) and immunostaining for the ION marker FOXP2 (E-H) on coronal sections at the level of r7/8. The rostral ION is absent in *Gli3*$^{xt/xt}$ mutants and the caudal ION is not organized into the typical layered pattern. Arrows indicate eMFN. 8 control and 8 mutant embryos were analyzed. (I-X) Coronal sections at the level of r7/8 hybridized for *Er81* (I-L, Q-T) or *Brn3.2* (M-P, U-X). *Er81* and *Brn3.2* expression marks different subsets of IMS/ION. *Er81*-positive cells show weak expression of *Brn3.2*. In the control hindbrain, *Er81*-positive cells have reached the ventral midline by E13.5. Arrowheads mark the IMS (I-P). In *Gli3*$^{xt/xt}$ mutants, *Er81*-expressing cells reach the ventral midline only at E14.5. Arrowheads mark the IMS (Q-X). Note that *Brn3.2* is also expressed in the AES and PES in controls (K), in the ectopic extramural stream (eES in S) and ectopic MF nuclei (eMFN in T). By E16.5 the ION has formed in both mutants and controls, but the ION is reduced in size and disorganized in *Gli3*$^{xt/xt}$ mutants as compared to controls. 4 control and 4 mutant embryos were analyzed at E13.5 and E14.5, 2 control an 2 mutant embryos were analyzed at E16.5. (Y) Quantification of the *Brn3.2*- and *Er81*-positive domain along the rostrocaudal extent of the ION in E15.5 coronal sections. Note that the rostral part of the ION is completely absent. The expression area was normalized for the size of the hemisphere at each level and is expressed in percent. Values are represented as mean ± SD. Levene´s test was used to assess equality of variances and an ANOVA one-way with a post-hoc Tukey test was used to test for significance. Hashtag indicates $p<0.05$ for size difference in the *Brn3.2* domain between control and mutant, asterisk indicates $p<0.05$ for the size difference in the *Er81* domain between control and mutant. n=4 brains, for both control and mutant. DAO: dorsal accessory olive, PO: principal olive, MAO: medial accessory olive. Scale bars: 200 µm.

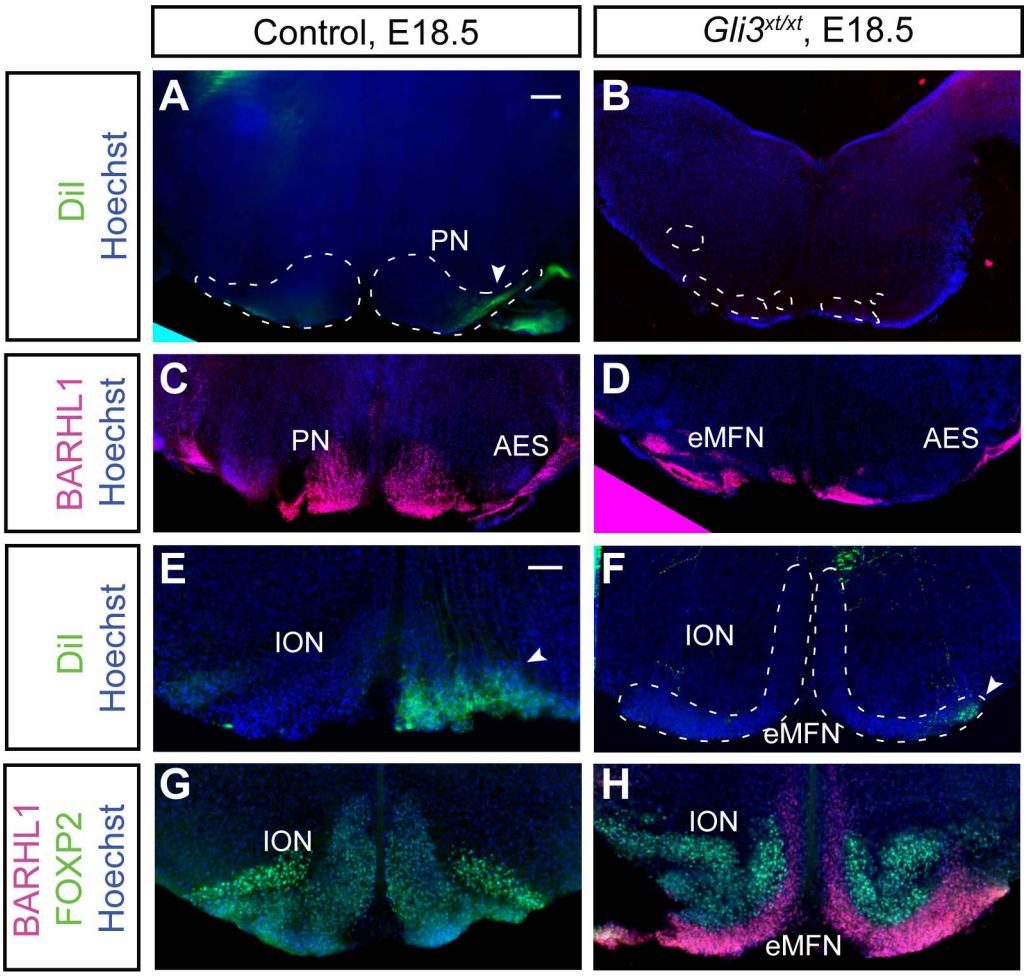

Figure S4: Retrograde tracing of mossy fiber and climbing fiber projections to the cerebellum. Hemicerebellar DiI injections to retrogradely label precerebellar nuclei in E18.5 control and *Gli3*$^{xt/xt}$ hindbrains (A, B, E, F). In the control, the contralateral pontine nucleus (PN, r4 in A) and inferior olivary nucleus (ION, r7/8 in E) are strongly labeled with DiI (arrowheads). In the *Gli3*$^{xt/xt}$ hindbrains, ectopic mossy fiber neurons (eMFN) at r5/6 and the ION are negative for DiI (B), though some sparse contralateral eMFN neurons are seen at r7/8 (F, arrowhead). The left side of each image is ipsilateral to the side of DiI injection. Note that the red fluorescent DiI signal was changed to green for better visualization. Adjacent sections show immunostaining for BARHL1 and/or FOXP2 to indicate the position of the ION and eMFN (C, D, G, H). 7 controls and 3 mutant embryos were analyzed. Scale bar: 200 µm (A – D), 100 µm (E – H).

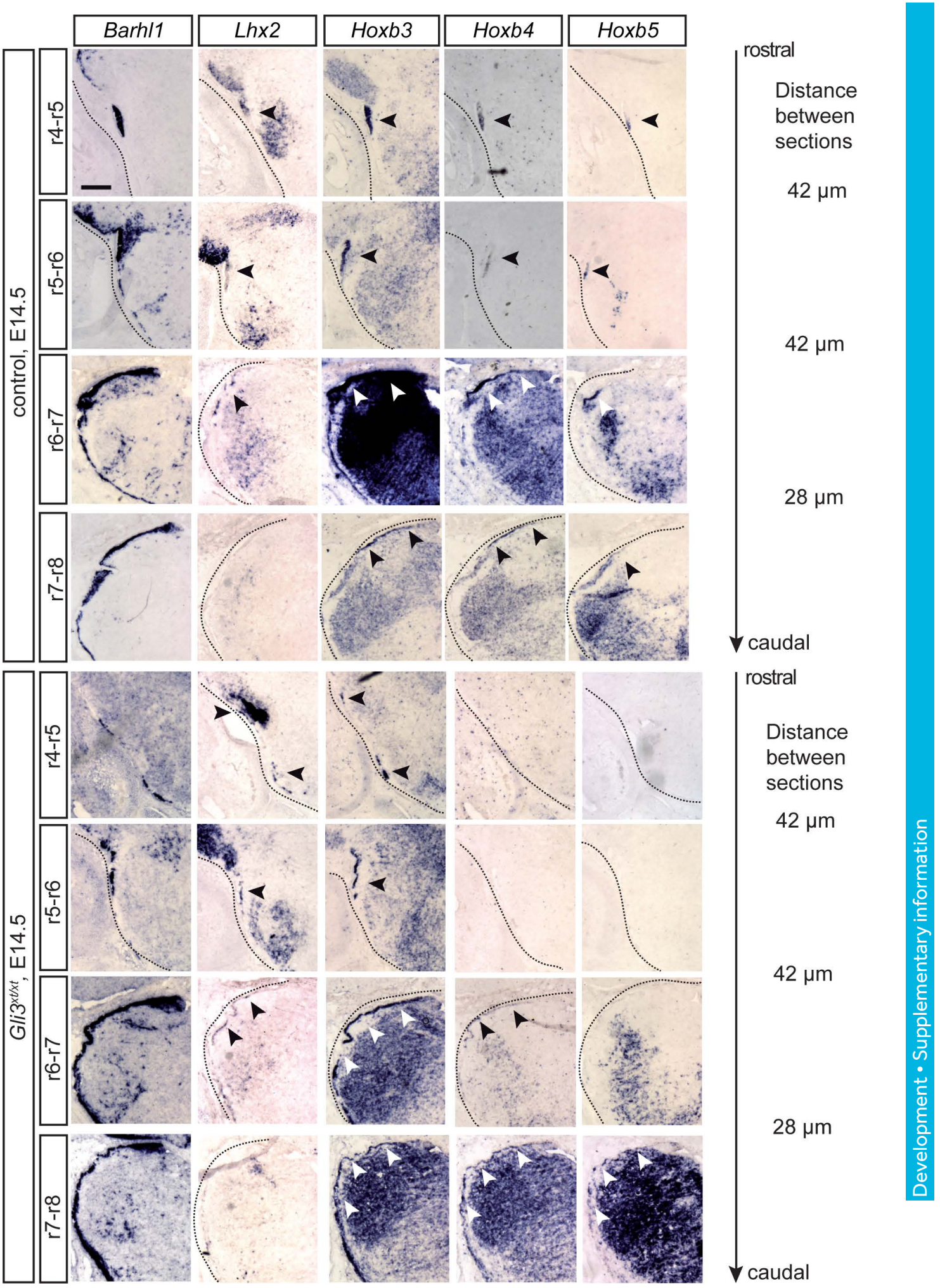

Figure S5: The r7 and r8-derived portion of the AES does not turn rostrally in the hindbrain of *Gli3*$^{xt/xt}$ mutants. *In situ* hybridization for *Barhl1, Lhx2, Hoxb3, Hoxb4* and *Hoxb5* on coronal sections at E14.5. Number of embryos analyzed: 5 controls, 4 mutants for *Lhx2*; 8 controls, 7 mutants for *Hoxb3/4/5*. Arrowheads indicate expression in AES. Scale bars: 200 µm.

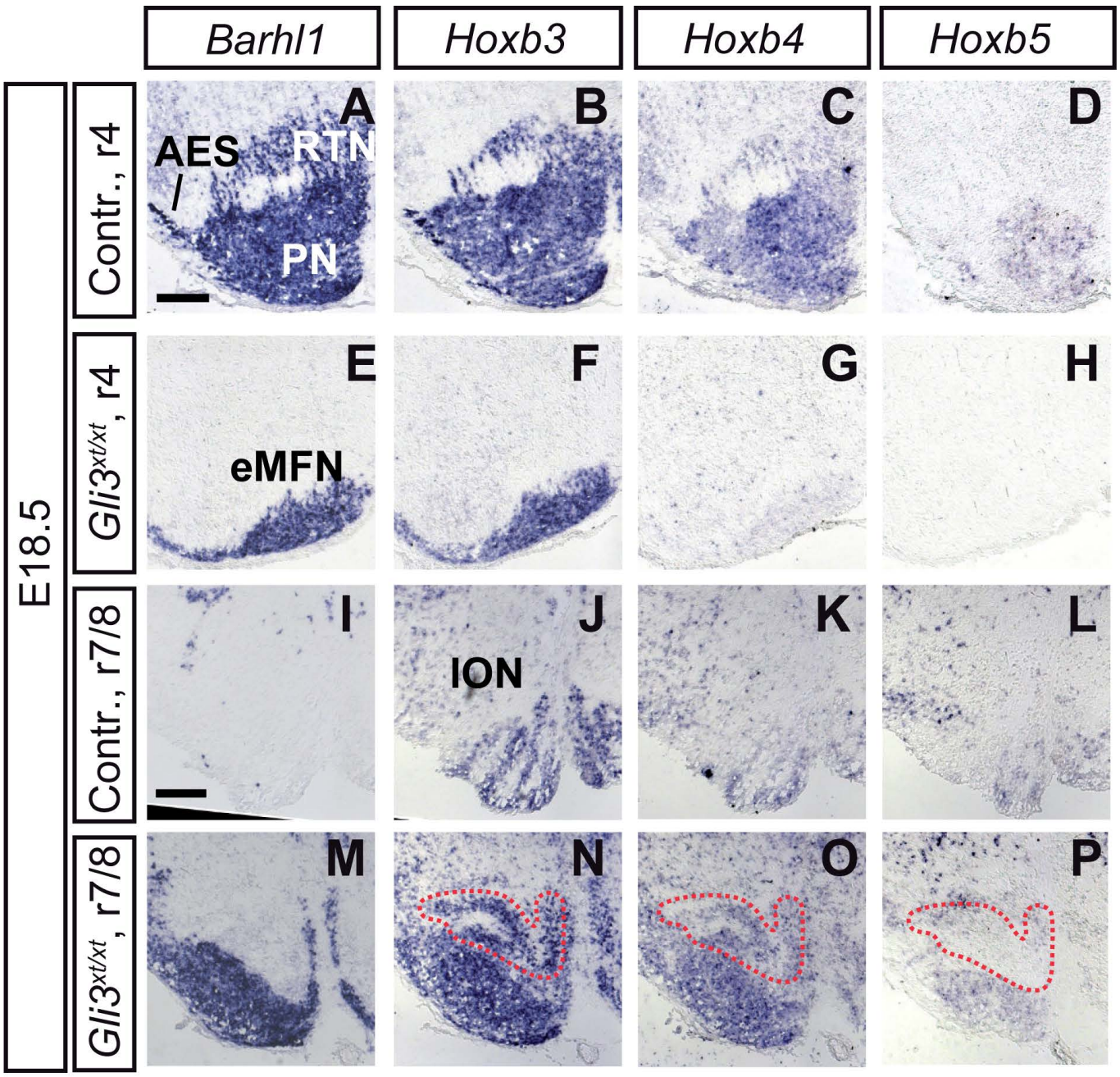

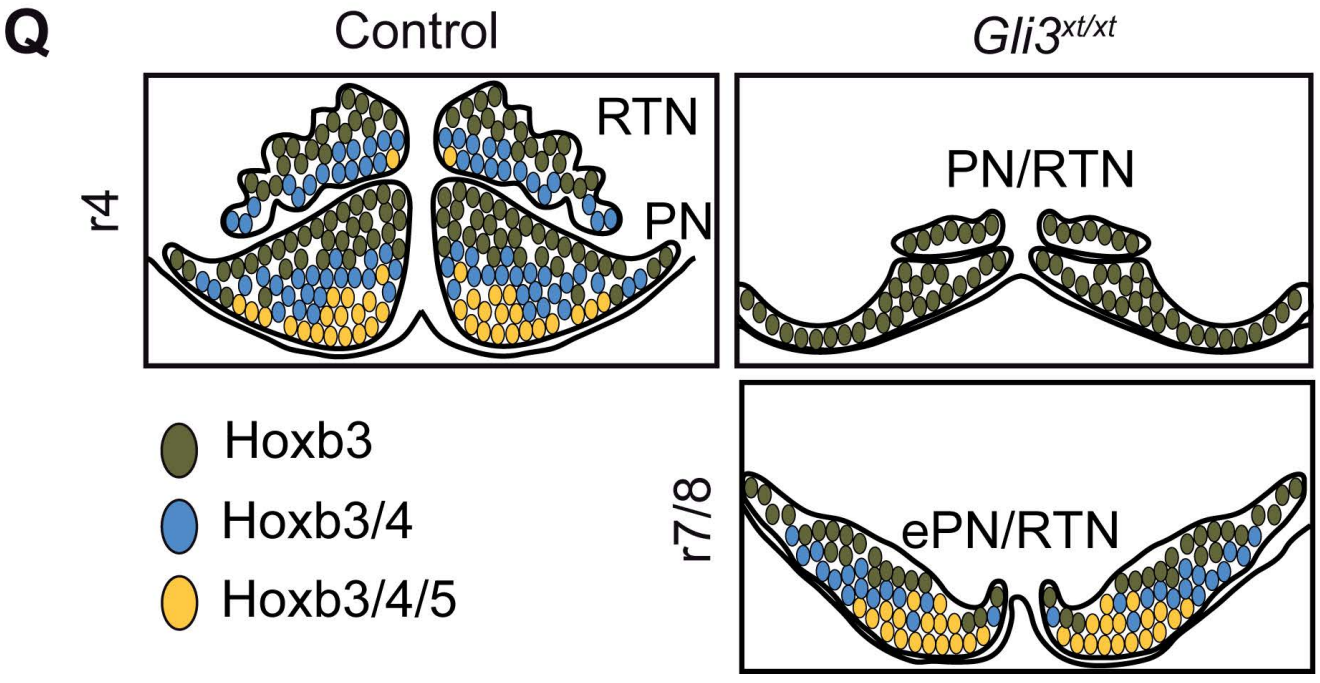

Figure S6: Expression of *Hoxb* genes in the PN/RTN and ION at E18.5. *In situ* hybridization for *Barhl1, Hoxb3, Hoxb4* and *Hoxb5* on coronal sections in r4 and r7/8. Note that the images of *Barhl1*-expressing nuclei are also shown in Figure 2 but are added here for easier comparison (A, E, I, M). In controls, the rostrodorsal PN expresses *Hoxb3*, the intermediate PN expresses *Hoxb3* and *Hoxb4* and the caudoventral PN expresses *Hoxb3, Hoxb4* and *Hoxb5* (A-D). In $Gli3^{xt/xt}$ mutants, the PN forming at the r4-r6 levels is negative for *Hoxb4* and *Hoxb5* (E-H) while the ectopic PN at the r7/8 level expresses all three *Hox* genes (M-P), in a pattern that resembles the Hox expression pattern of the PN in controls. All three Hox genes are also expressed in the ION in controls and $Gli3^{xt/xt}$ mutants (I-P, ION outlined in dotted red line). (Q) Schematic summarizing the *Hoxb* expression patterns in the PN/RTN. Number of embryos analyzed: 3 controls, 4 mutants. Scale bars: 200 μm.

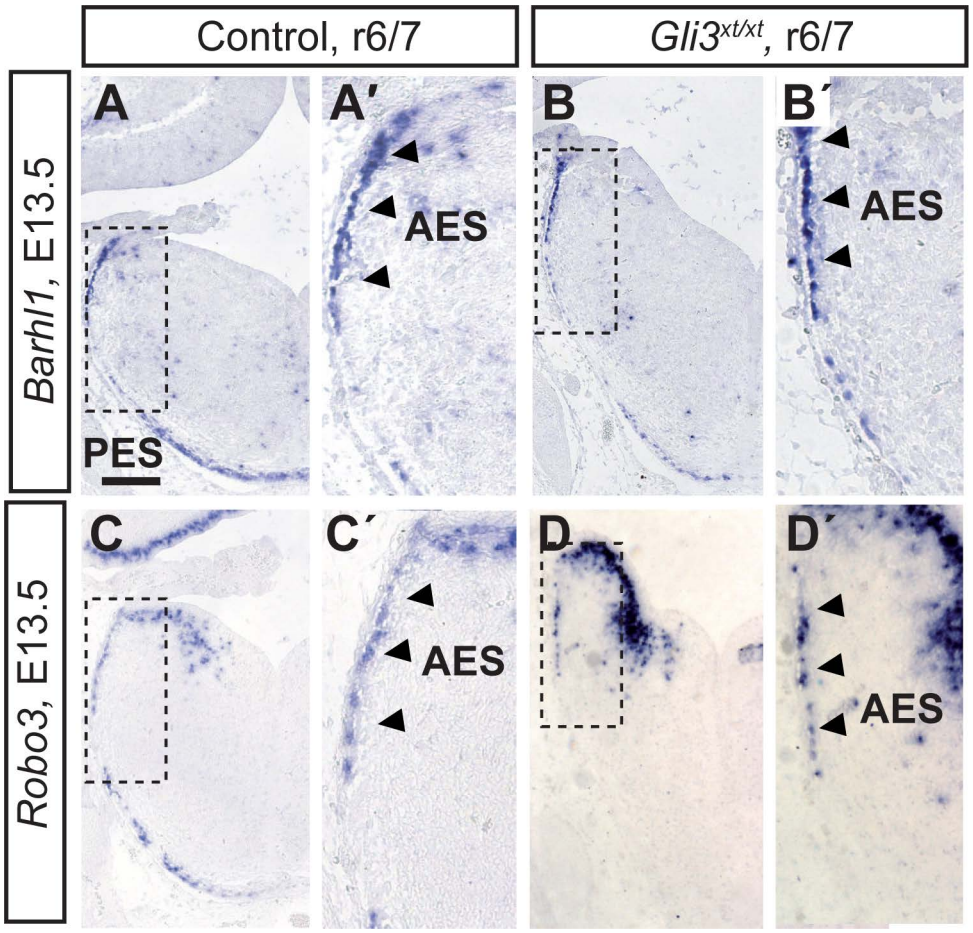

Figure S7: Expression of *Robo3* in the E13.5 hindbrain in controls and *Gli3*$^{xt/xt}$ embryos. *In situ* hybridization for *Barhl1* and *Robo3* on coronal sections. (A′-D′) Higher magnification of the boxed areas in A-D. *Robo3* is expressed in the AES in controls and *Gli3*$^{xt/xt}$ mutants. Number of embryos analyzed: 3 controls, 3 mutants. Scale bar: 200 µm (A-D).

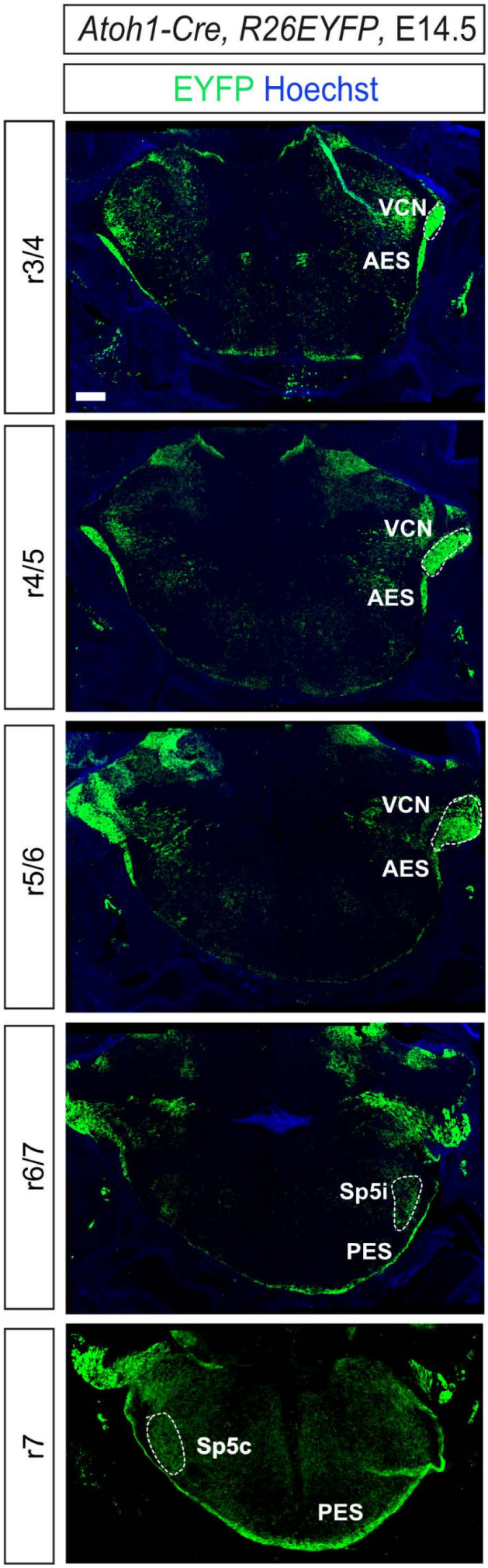

Figure S8: *Atoh1-Cre* induced recombination pattern in the E14.5 hindbrain of control embryos (Genotype: *Atho1-Cre, R26*$^{EYFP/+}$). Immunostaining for EYFP on coronal sections, rostrocaudal levels are indicated. AES, PES, and ventral cochlear nucleus (VCN) are derived from the *Atoh1*-lineage. The *Atoh1*-lineage also contributes neurons to the intermediate and caudal spinal trigeminal nucleus (Sp5i and Sp5c). n=4 embryos. Scale bar: 200 μm (A-D).

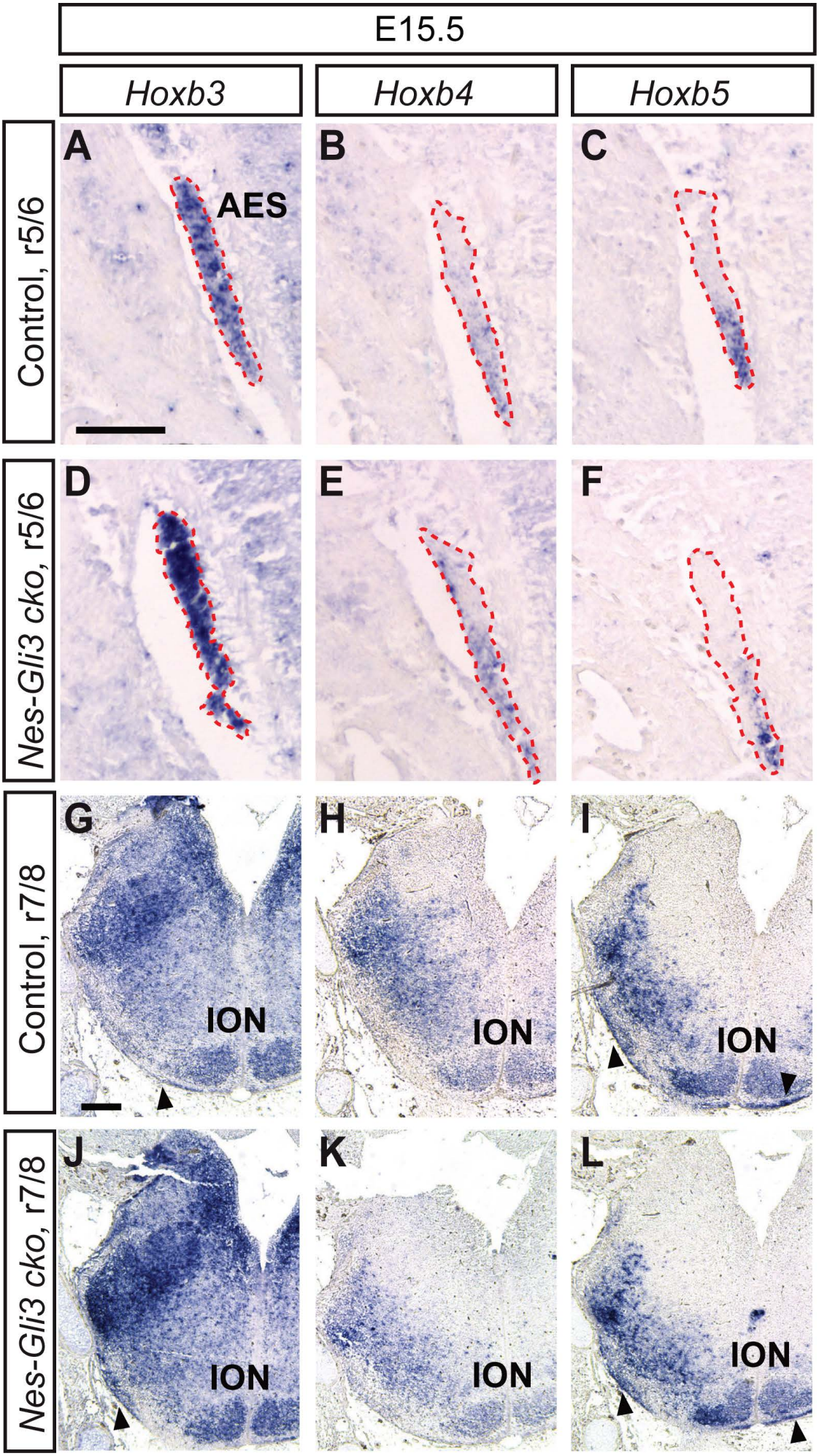

Figure S9: *Hoxb* gene expression is not altered in AES, PES and ION in *Nes-Gli3 cko* embryos. *In situ* hybridization for *Hoxb3, Hoxb4* and *Hoxb5* on E15.5 coronal sections. (A-F) AES is outlined with red dotted line. (G-L) Arrowheads indicate PES. Number of embryos analyzed: 3 controls, 3 mutants. Scale bars: 100 μm (A-F); 200 μm (G-L).

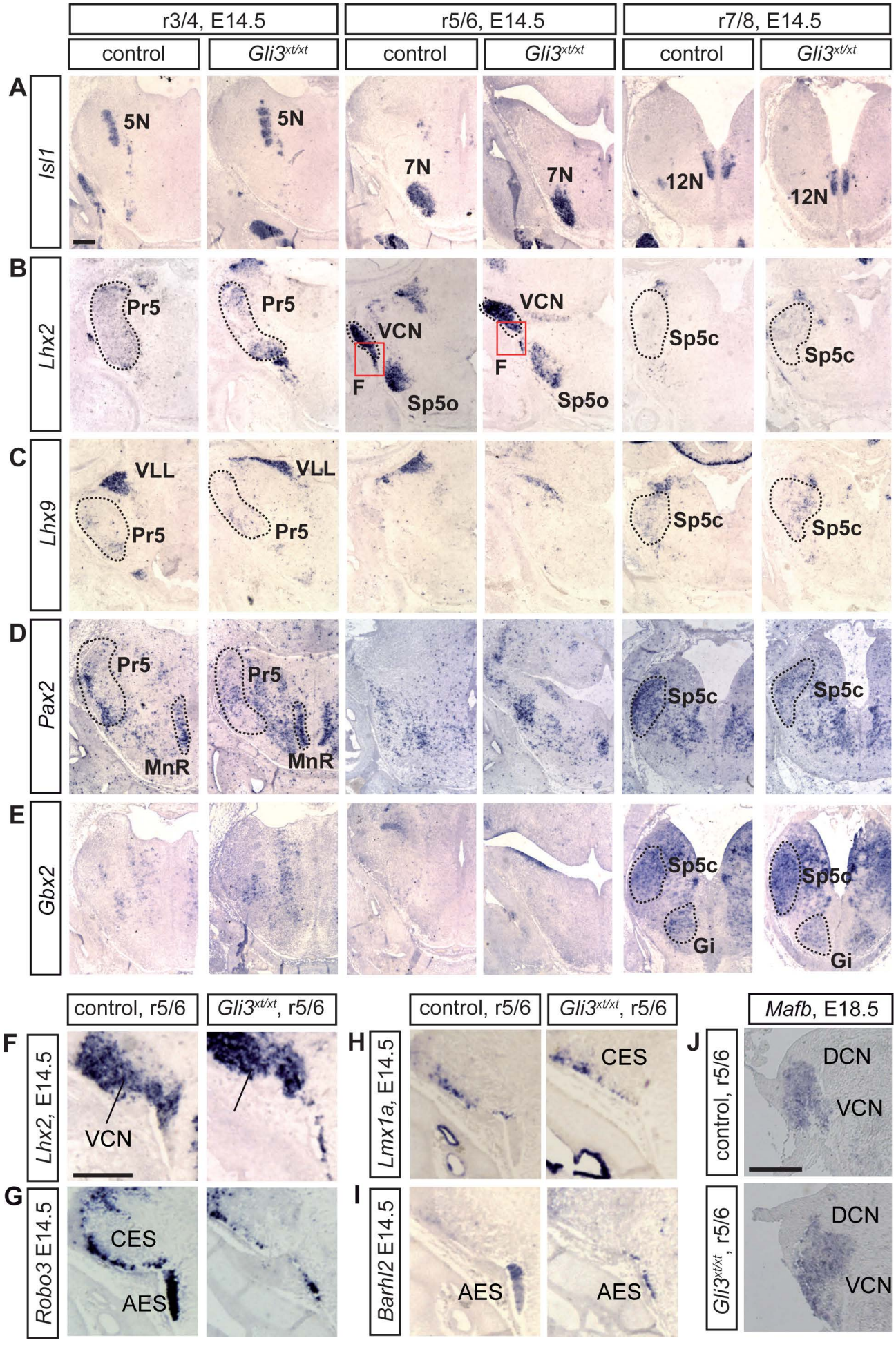

Figure S10: Analysis of non-precerebellar hindbrain nuclei in *Gli3*$^{xt/xt}$ mutants. Coronal sections of control and mutant hindbrain at the level of r3/4; r5/6 and r7/8 hybridized for various *RNA in situ* probes, as indicated. (A) *In situ* hybridization for *Isl1* showing that the motor nuclei of the cranial nerves are present in *Gli3*$^{xt/xt}$ mutants. 8 control and 8 mutant embryos were analyzed. (B) *Lhx2* is expressed in the principal sensory trigeminal nucleus (Pr5), the oral and caudal divisions of the spinal trigeminal nucleus (Sp5o and Sp5c, respectively) and the ventral cochlear nucleus (VCN) in control and mutant hindbrain. 5 control and 4 mutant embryos were analyzed. (C) *Lhx9* is expressed in the Pr5, ventral lateral lemniscus (VLL) and in the Sp5c in control and mutant hindbrain. 2 control and 2 mutant embryos were analyzed. (D) *Pax2* is expressed in the Pr5, median raphe nucleus (MnR) and Sp5c in control and mutant hindbrain. 3 control and 3 mutant embryos were analyzed. (E) The expression pattern of *Gbx2* in the Sp5c and gigantocellular reticular nucleus (Gi) is comparable in in control and mutant hindbrain. 2 control and 2 mutant embryos were analyzed. (F-K) The cochlear extramural stream (CES, *Robo3* and *Lmx1a* positive in G and H, respectively) and VCN (*Lhx2* and *Mafb* positive in F and J, respectively) in the *Gli3*$^{Xt/Xt}$ hindbrain are comparable to the CES and VCN in controls. The *Barhl2* positive AES (I) is clearly separated from the CES (G,H) in both control and mutant hindbrain and the VCN is comparable to controls (J). 5 control and 4 mutant embryos were analyzed for *Lhx2* and *Barhl2*; 3 controls and 3 mutants for *Robo3*; 4 controls and 4 mutants for *Lmx1a*; 3 controls and 3 mutants for *Mafb*. 5N, motor trigeminal nucleus; 7N, facial nucleus; 12N, hypoglossal nucleus; DCN, dorsal cochlear nucleus. Scale bar: 200 µm.

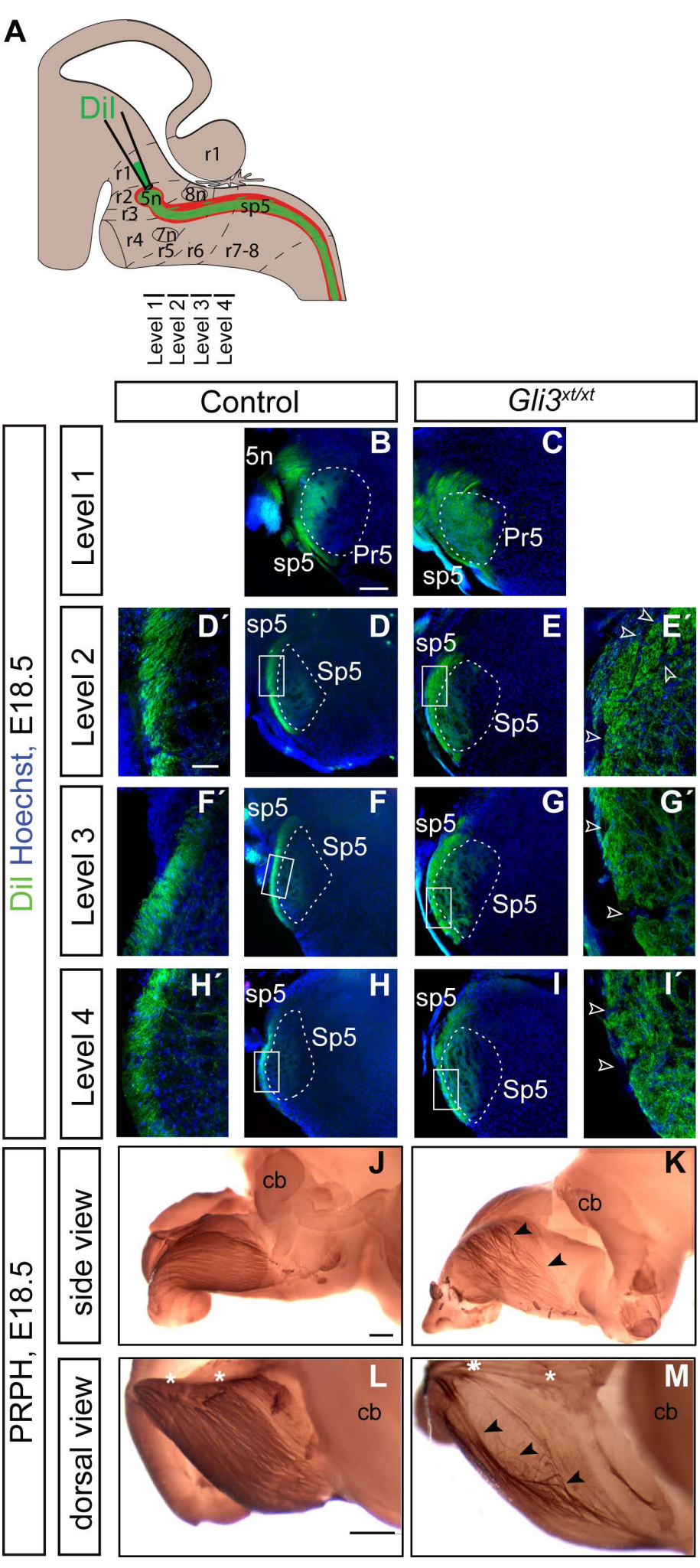

Figure S11: Disorganization of the spinal trigeminal tract in *Gli3*$^{Xt/Xt}$ mutants. (A-I) Anterograde tracing of central trigeminal projections by injecting DiI into the trigeminal ganglia (5Gn) of E18.5 control and *Gli3*$^{Xt/Xt}$ mutants. (A) DiI diffusion results in labeling of ascending tract axons innervating the principal trigeminal nucleus (Pr5) and of descending projections forming the spinal trigeminal tract (sp5), which innervate the spinal trigeminal nucleus (Sp5). The rostrocaudal levels shown in B-I are indicated. (B-I) In the control, the sp5 tract is a compact axonal bundle that sends perpendicular projections into the barrelette neurons of the Pr5 (B) and Sp5 nuclei (D, F, H). In the *Gli3*$^{Xt/Xt}$ mutants the sp5 tract is defasciculated (arrowheads in E´,G´,I´) and the projections into the barrelettes of the Pr5 and Sp5 are disorganized (C, E, G, I). D´ - I´ are maximum intensity projections of Z-stacks acquired with structured illumination; areas are indicated in D-I. Note that the red fluorescent DiI signal was changed to green for better visualization. n=8 controls, n=2 *Gli3*$^{Xt/Xt}$ mutants. (J-M) Whole-mount immunostaining for peripherin (PRPH) to visualize the trigeminal tract shows the disorganization of the tract in *Gli3*$^{Xt/Xt}$ mutants. Side view (J,K) and dorsal view (L,M). Asterisks indicate the dorsal midline. Note that the images are composed of several stitched images to have the entire hindbrain in focus. n=4 controls, n=2 mutants. Scale bars: 200 µm (B-M), 50 µm (D´-I´).

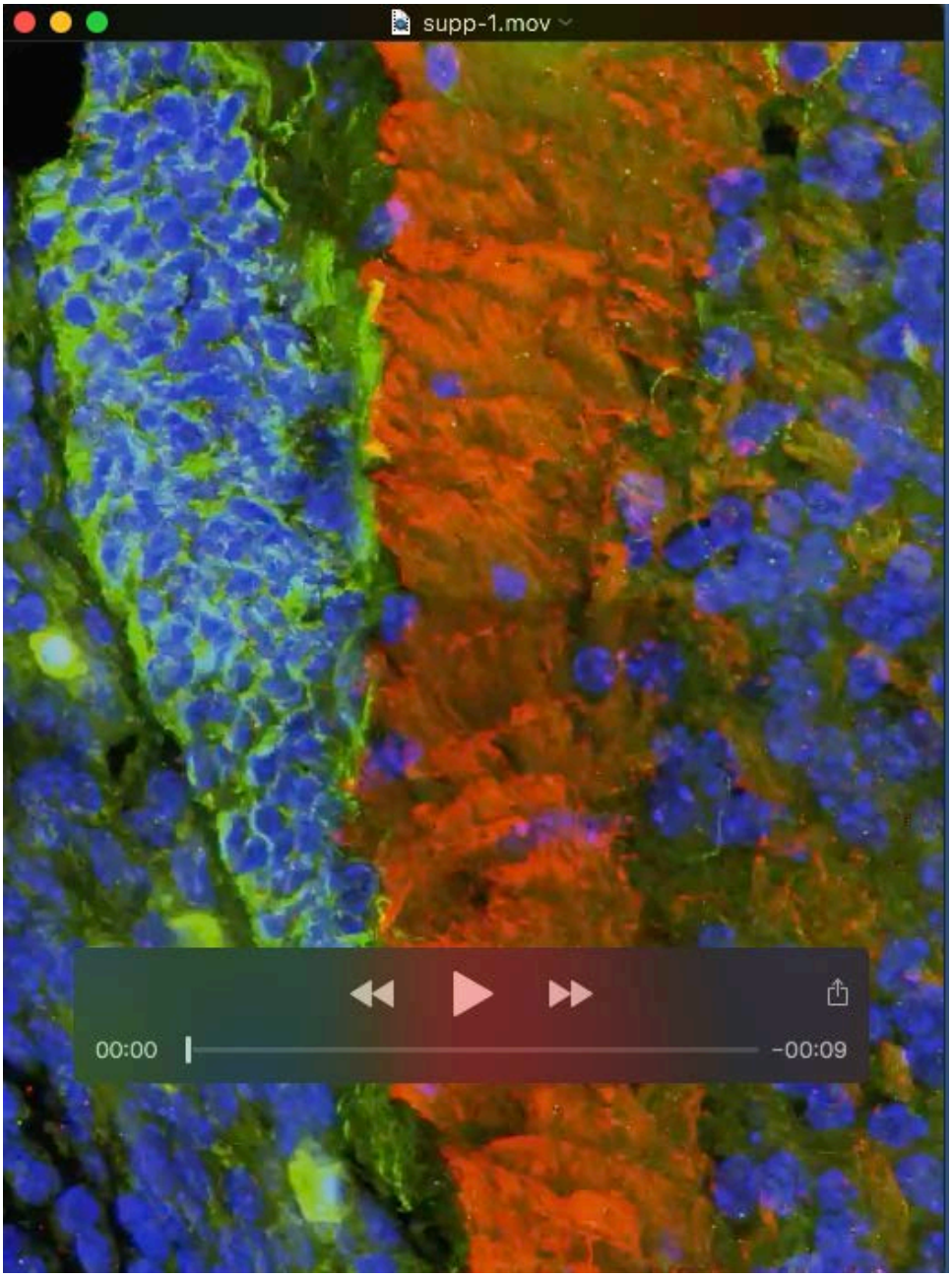

Movie 1: Ventral AES cells are in close contact with the sp5. 3-D projection of a Z-stack of the image shown in Figure 8 K2. Immunostaining for PRPH (red) and DCC (green). Hoechst is in blue. Z-stack was acquired with structured illumination.